Synthesis of MXene-Epoxy Nanocomposites

A thesis
submitted to the Faculty
of

DREXEL UNIVERSITY

by
Jay B. Shah

in partial
fulfillment of the
requirements for the degree
of

Master of Science in Materials Science and Engineering
June 2017

Dedication

To my late grandfather

Shantilal Nanchand Shah

1937 – 2015

Acknowledgements

As I put the finishing touches on my Master's Thesis, I cannot but think of the countless individuals to whom I owe a debt of gratitude. I just wanted to mention my sincere acknowledgements to these individuals below. I would like to express my forgiveness beforehand, if any names are unintentionally absent.

First, I want to thank my advisor Prof. Yury Gogotsi for having me in his lab for the last 4 years, from the time I began working in the lab as a STAR student to my time as a Master's student. Dr. Gogosti's tireless passion for science and discovery is an inspiration. I learned numerous things by working for him, not limited to just materials science and nanotechnology, but also about how to conduct research and present it. The opportunity to work in his research group, along with the excellent graduate students, post-docs and other members in his group, has thoroughly enriched my experience at Drexel. I also want to thank Drs. Michel Barsoum and Caroline Schauer for serving on my Defense Committee. I previously worked for Dr. Barsoum, and would like to thank him for that opportunity as well.

I want to thank the mentors I have had at my time at Drexel, and in DNI, including Michael Naguib, Olha Mashtalir and Babak Anasori. I would be half the researcher I am today if not for their guidance, help and critical comments. In particular, Babak was instrumental in guiding me through the last 2 years relating to my Master's Thesis work. The many discussions I had with him about results, along with his critical comments and encouraging words, have been invaluable.

I want to express my gratitude to Prof. Guiseppe Palmese. We collaborated with Dr. Palmese and Dr. Santosh Kumar Yadav, who works in his lab, to study epoxy composites of MXenes. Their expertise and guidance was crucial for introducing me to epoxies, for planning experiments I carried out, and for understanding results. I want to thank them for all their help. I also want to thank the other colleagues I worked with for this project. This work would not have been possible without all the help that Christine Hatter provided me, both in terms of characterization results but also experiment planning. This work was enhanced by the help of Bilen Akuzum who provided viscosity measurements.

In addition, I am very grateful to the many present and past members of DNI, including co-op students, graduate students, post-docs, visiting researchers and staff, whose time at Drexel coincided with mine. I did not have the good fortune to collaborate with many of these excellent researchers at DNI, but I nonetheless want to thank them for their camaraderie. The countless lab meetings taught me a great deal about materials science and also about scientific research. In particular I want to mention these people for their help, comments, and friendship: Mohamed Alhabeb, Muhammad Boota, Narendra Kurra, Kanit Hantanasirisakul, Tyler Mathis, Kathleen Maleski, Katie Van Aken, and Bernard Haines.

Lastly, I want to thank and acknowledge my parents, my grandparents, my brother, my aunts and uncles, my cousins, and my friends for their love, support, guidance, and good wishes. I am eternally indebted to them.

TABLE OF CONTENTS

List of Tables

LIST OF FIGURES

Abstract

Synthesis of MXene-Epoxy Nanocomposites

Jay B. Shah

Advisor: Prof. Yury Gogotsi

This thesis explores the synthesis of MXene-epoxy nanocomposites. MXenes are a family of two-dimensional materials which display versatile chemistries that allow the material to be tuned for applications that include electrochemical storage devices, electromagnetic interference shielding devices, and catalysts, to name a few. Composites of MXenes with a variety of polymers have been produced, and they show enhanced mechanical and electrical properties. In this work, epoxy composites with MXenes are synthesized, because the use of a platelet-like filler allows property enhancements such as 2D stress transfer, and the formation of diffusion barriers and percolating thresholds. Complete exfoliation of the multilayered MXenes into their 2D sheets is desired in order to realize these property improvements.

Two different techniques of producing MXene-epoxy composites are evaluated. The first is a tradition *in situ* polymerization technique, which involves the dispersion of the filler in a volatile solvent. Acetone was used to disperse Ti_3CNT_x into single layers, before the dispersion was mixed with epoxy. The other technique involves the application of laminar shear stress on multilayered $Ti_3C_2T_x$ particles, in order to exfoliate them into single layers dispersed in the epoxy matrix. In this system, a room temperature ionic liquid (RTIL) is used as the dispersant for the filler and the initiator for epoxy cure. The problems associated with MXene exfoliation, nanoparticle dispersion, and nanocomposite

synthesis are considered while evaluating these methods of synthesizing these composites.

It was found that while a few single layers of Ti_3CNT_x were successfully exfoliated, a majority of the particles were still multilayered. The physical performance of the composite was lackluster as a result of this poor exfoliation and dispersion. The lack of covalent bonding between Ti_3CNT_x and epoxy, and the lack of wettability of the filler are also areas of concern. In the $Ti_3C_2T_x$-epoxy-RTIL composites, the exfoliation of single layers was also not accomplished. Despite approximate shear stresses experienced by the particles being higher than the theoretically predicted interlayer coupling, stacked $Ti_3C_2T_x$ particles were observed. Instead, the $Ti_3C_2T_x$ particles had undergone swelling, which resulted from the intercalation of the RTIL. Upon application of sufficient shear stress, intercalation of bigger molecules was observed. Better properties were also obtained, leading us to hypothesize that epoxy intercalation has occurred. The reasons for poor exfoliation and poor dispersion are detailed, and future areas of study for better understanding of the MXene-epoxy system are proposed.

1. Introduction

1.1 Motivation and Approach

This thesis investigates the synthesis of MXene-epoxy nanocomposites. MXenes are a family of two-dimensional crystals with high aspect ratios. Like other 2D materials, many applications of these materials have been investigated, ranging from electrochemical storage devices to reinforcement in composites. Epoxy composites made with 2D materials are predicted to have superior mechanical, thermal and electronic properties. As of 2017, I am not aware of any reports on the synthesis or properties of MXene-epoxy composites. Composites of MXenes with other polymers have been made, and show improved mechanical and electrical properties. Interesting chemistries and potential applications have been found for these MXene composites. With this in mind, the processing of MXene-epoxy composites has been studied in this work.

Attempts were made especially to produce these composites via methods that are scalable and simple. MXene exfoliation into single layers and their dispersion are of particular importance in order to fully realize the potential of the composite material. Cost-effective methods and scalable methods of delaminating MXene single layers from their multilayered precursors are necessary if they are to be used widely. Similarly, a good dispersion of MXenes in composites is required for mechanical reinforcement and transport property modifications. In this study, both traditional amine curing agents and novel room temperature ionic liquid hardeners have been used for the synthesis of MXene-epoxy composites.

1.2 Background

1.2.1 Epoxy Chemistry

Epoxies are a type of thermosetting polymer in which a 3-D cross-linked network is formed.[1] Covalent bonds between the epoxy monomers are formed after curing, creating a solid material that cannot be remolded.[2] The mechanical, thermal and chemical properties of this material can be tuned by changing the monomers, changing the extent of network formation, or adding reinforcement phases. Figure 1.1 shows three monomeric or oligomeric epoxy structures that are based on bisphenol or polyphenolic structures. Bisphenol-based epoxy monomers are the most common, as they have a low viscosity for processing, along with high crosslinking density and stiffness. Of particular interest in this thesis is the Diglycidyl Ether of Bisphenol A (DGEBA) oligomer, seen in Fig 1.1(A). Some other thermosetting polymers are vinyl esters and polyurethanes. Thermosetting resins are widely used today as the matrix for fiber-reinforced composites for high performance structural applications. They are also used as adhesives to provide bonding between complex parts, or as high performance coatings due to their thermal and chemical resistance.

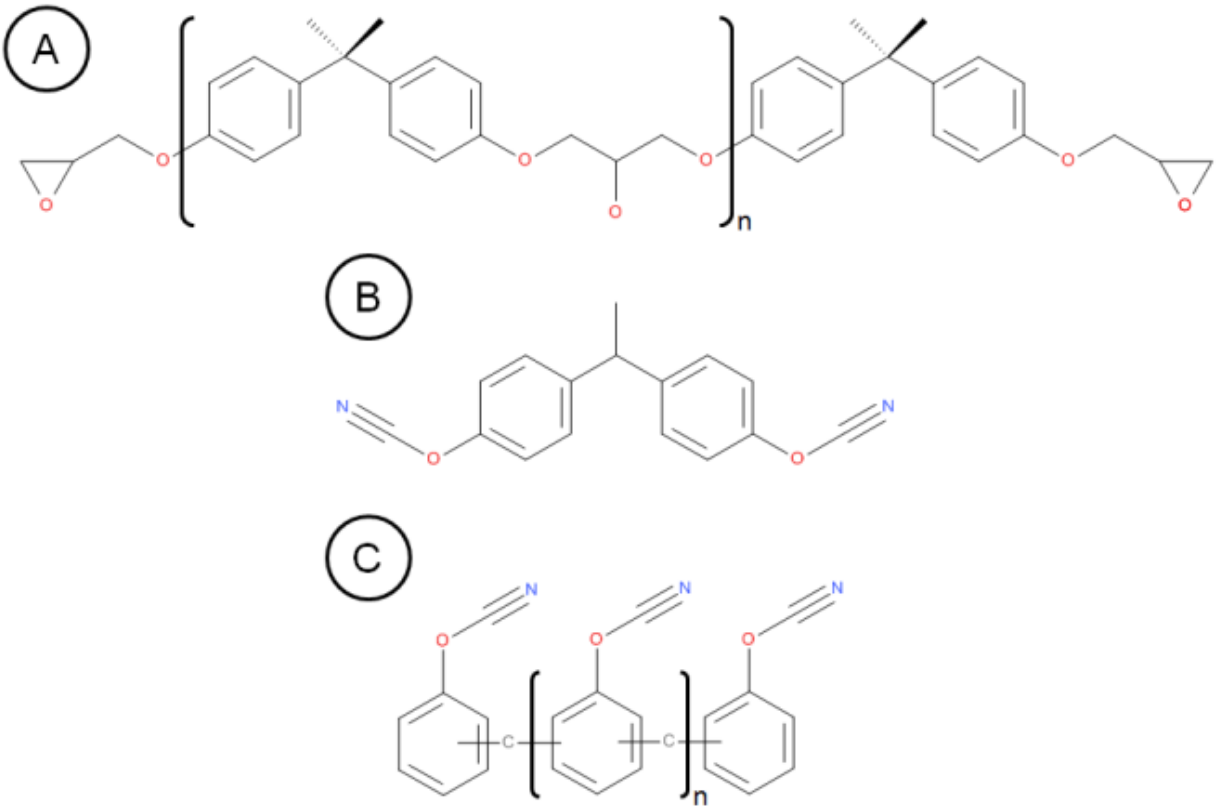

Figure 1.1: (A) Diglycidyl ether of bisphenol A (DGEBA, tradename: EPON 828), (B) Dibsphenol E Cyanate Ester (tradename: Primaset LECY), and (C) oligo(3-methylene-1,5-phenylenecyanate ester) (tradename: Primaset PT-30). Adapted with permission from [3].

The reaction of epoxies occurs via nucleophilic addition reactions that cleave the oxirane ring.[4] The two reaction mechanisms that can accomplish this are seen in Figure 1.2. The first reaction pathway is step growth polymerization in which the epoxy monomers react with primary and secondary amines. The epoxy-amine ratio is critical in order to create the most optimum structure. Excess epoxy or hydroxyl impurities can result in competing etherification reactions that decrease crosslinking density and the glass transition temperature (T_g). The second reaction mechanism is chain extension polymerization promoted by a cationic initiator, which initiates the anionic opening of the epoxide ring. In this mechanism, there is no optimum hardener-epoxy ratio. But the

concentration of the hardener used will affect the material properties, as the average molecular weight between crosslinks will decrease as hardener concentration increases. Figure 1.2(A) shows the step growth polymerization of epoxy monomers, and (B) shows the chain extension mechanism of forming a crosslinked epoxy network.

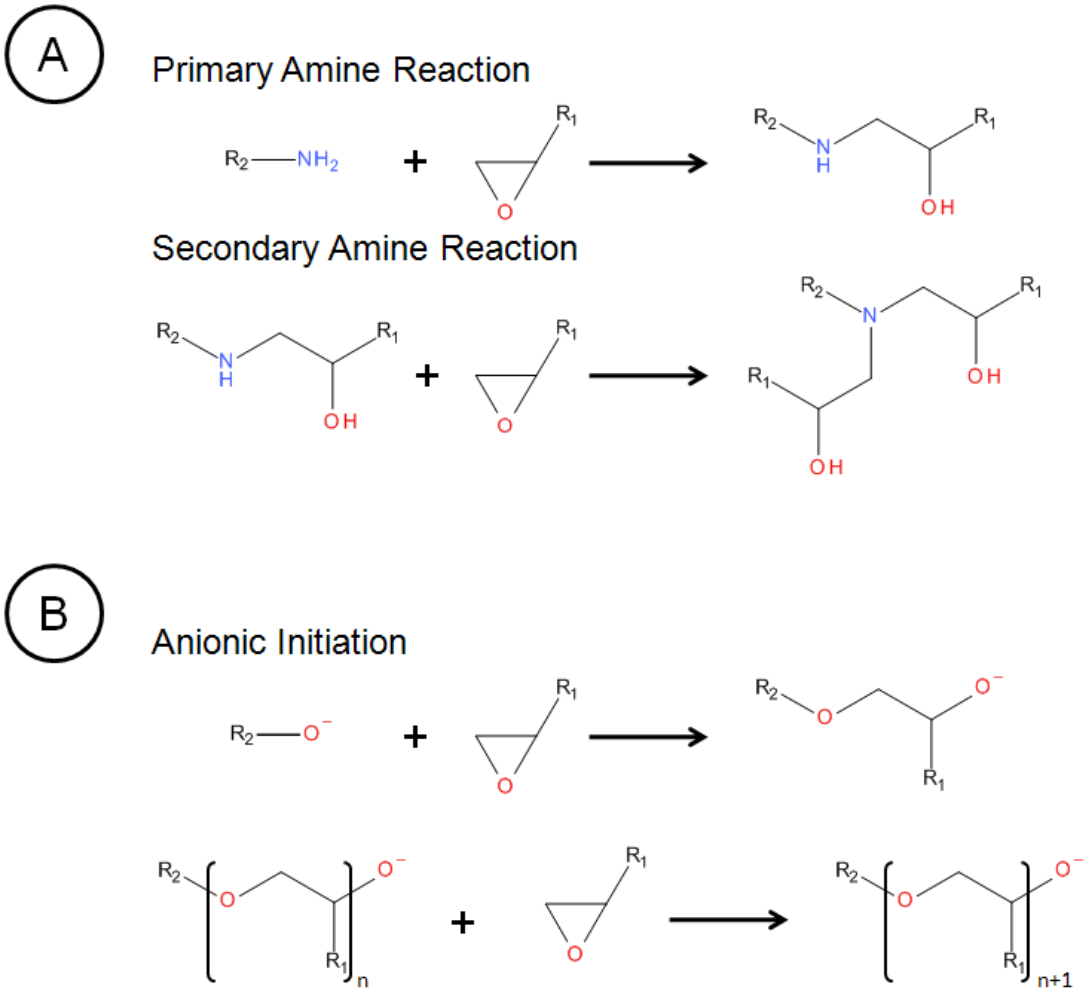

Figure 1.2: (A) Step-growth polymerization of epoxy carried out by a primary or secondary amine, and (B) anionic initiation of the chain extension of epoxy. Adapted with permission from [3]. Epoxy monomers with more than one oxirane ring produce a thermoset network.

One class of compounds which have demonstrated the ability to initiate chain extension of epoxy monomers are imidazolium-based room temperature ionic liquids (RTIL).[5.6] These compounds are a class of salts that remain molten at room temperature because of their irregular structure and large ionic size.[7,8] The asymmetrical, irregular shape of the salt molecules means that crystal packing is prevented.[9] The large ionic size means that they have a large ionic-association length that decreases the lattice energy.[10] Most RTILs consist of a heterocyclic cation and an inorganic anion. The ionic nature of these chemicals means there are both anionic and cationic sites that can allow for chemical processing, reaction chemistry or catalysis.

In this thesis, both step growth and chain extension polymerization of epoxies has been used to synthesize epoxy nanocomposites. The RTIL, 1-ethyl-3-methyl imidazolium dicyanamide (EMIM-DCN) has been investigated to promote the chain extension mechanism. Figure 1.3 shows the mechanism by which EMIM-DCN initiates epoxy chain extension. This reaction consists of two adducts and two etherification reactions.[3,11] A carbene forms on the imidazolium ring, with its positive charge stabilized by the dicyanamide anion. The structure of the anion remains intact throughout the reaction. The carbene begins the anionic opening of the oxirane ring, which creates an anionic adduct structure. The adduct reacts similarly with other epoxy monomers or chains initiating the chain extension step. EMIM-DCN is particularly interesting to cure epoxies because it is a latent curing agent. It is miscible in the DGEBA epoxy resin, and can initiate cure only at elevated temperatures (T>80°C).[5] The mixture of this RTIL and DGEBA can remain stable in liquid form for many months at ambient conditions. The broad processing window of this mixture makes it of interest for applications requiring long shelf lives

such as filament winding or adhesives. Moreover, EMIM-DCN has shown the ability to disperse silica[12], graphite nanoplatelets[12] and carbon nanotubes[12,13], which allows the processing of nanocomposites with increased efficiency. The mixture of DGEBA and EMIM-DCN has also been used to mechanically exfoliate graphite to form graphene-epoxy nanocomposites.[14]

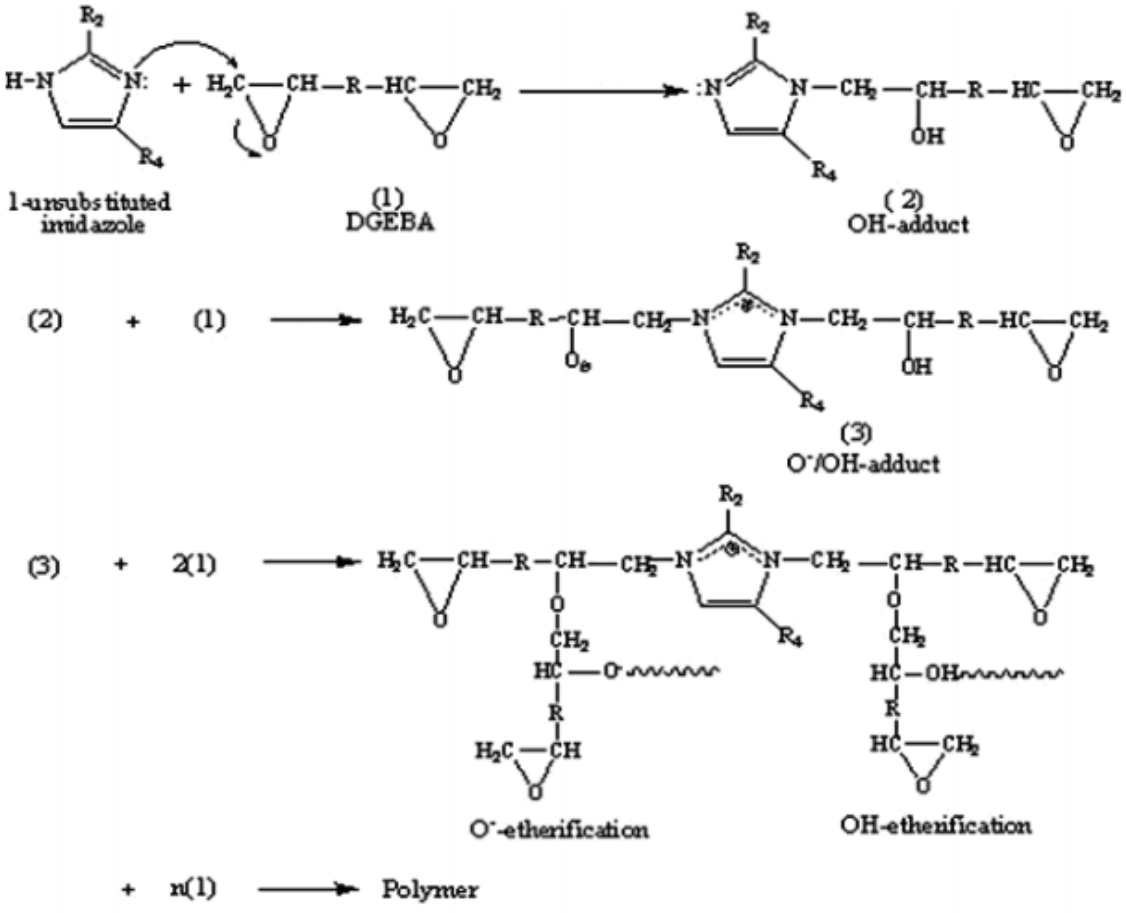

Figure 1.3: Chain polymerization of DGEBA by an imidazolium dicyanamide based. Adapted with permission from [11].

1.2.2 Nanocomposites

Polymer nanocomposites contain inorganic particles that have high aspect ratios, and at least one dimension that is in the lengthscale of 1-100 nanometers.[15] The nanocomposites potentially offer enhanced electrical, mechanical and thermal properties.[16] The filler particles in nanocomposites do not extend continuously all throughout the composite part, unlike in conventional fiber-reinforced composites.[17] This limits their potential for mechanical reinforcement. However, more fundamental improvements of the matrix are possible due to their small size. The exceptional properties of nanometer-sized materials, the modification at the polymer-particle interfacial region of the polymer network, and the formation of percolation structures allow nanocomposites to exhibit property enhancements.

The addition of nanoparticles modifies the mechanical properties of the matrix, with reinforcement dependent on particle geometry[18], nanoparticle dispersion[19] and interfacial stress transfer[20]. The reinforcement potential of nanoparticles is limited as a result of the morphology of their distribution, because it is not continuous like in traditional fiber-reinforced composites. Nonetheless, improved tensile modulus[21] and fracture toughness are observed[22,23]. The high surface area to volume ratio of nanoparticles allows increased fracture toughness by mechanisms such as crack bridging[24], crack deflection[25,26], crack pinning[27], or plastic void growth[26]. Other properties such as coefficient of thermal expansion and thermal stability are also enhanced because of the addition of stiff nanoparticles. Moreover the properties of nanocomposites are modified as a result of the formation of percolation or barrier networks that control transport properties. Epoxies, like other thermosets, are electrical

insulators with moderate thermal transport coefficients. The addition of high-aspect ratio nanoparticles offers alternate transport pathways via the formation of percolating networks of highly conductive filler.[28] The quality of filler dispersion and filler geometry affects this network. Meanwhile, plate-like particles form diffusion barriers which decrease the diffusion rates of liquids and vapors.[29,30]

1.2.3 Nanoparticle selection

Nanoparticles come in varying dimensions: rod-like (1D), plate-like (2D), and particulate (3D). The aspect ratio and geometries of these types of nanoparticles affects the type of property improvements, mechanical reinforcement, and type of network formed when used to make composites.

One-dimensional rod-like particles, similar to fibers in conventional fiber-reinforced composites, offer improved stress transfer efficiency. They also reach their percolation threshold, above which long-range connectivity exists, at lower volume fractions as compared to other geometries. The composites made from these fillers also show enhanced toughness behavior as a result of crack bridging during fracture. Some examples of rod-like nanoparticles are cellulose nanofibers[31,32,33] and carbon nanotubes[34,35]. Cellulose fibers have a polymer miscible interface, and hence are used for mechanical reinforcement. Carbon nanotubes provide increased fracture toughness and electrical conductivity at low volume fraction loading. The limitation of using rod-like nanoparticles is the problem of their dispersion in polymers, which is complicated by

clumping and entanglement, and thus physical processing and favorable solvent chemistry is required for processing.

Plate-like, two-dimensional nanoparticles also form a percolating threshold at relatively low volume fractions.[36] They possess unusual electronic, mechanical and optical properties, and hence have been studied extensively in a wide variety of applications.[37-42] In nanocomposites, two-dimensional stress transfer and diffusion barriers are the benefits of the addition of this type of filler. Examples of plate-like nanoparticles are smectite clays[29,30,43] and graphene or few-layer graphite nanocomposites[44,45,46,47]. Graphite has been used as filler for polymer composites[48] even before graphene was discovered in 2004[49]. The discovery of graphene has accelerated research on their use in producing nanocomposites. Smectite clay nanocomposites offer enhanced mechanical properties such as Young's modulus and tensile strength, with other properties such as fire retardancy, barrier resistance, and ionic conductivity also showing improvement. Similarly, graphene nanocomposites demonstrate some of the improved properties of the clay nanocomposites, along with having high electrical conductivity. Issues encountered during the processing of 2D materials in composites are the problem of dispersion, and the problem of exfoliation into single- or few-layered flakes. Intercalation chemistry or physical exfoliation methods need to be used to exfoliate these nanoparticles.

Lastly, 3-dimensional particulates have also been used to make nanocomposites. They have an aspect ratio approximately equal to 1, and hence only form a percolation network at high volume fraction loading. This limits enhancements to transport properties. But mechanical properties such as stiffness and toughness are enhanced as

crack propagation is arrested, such as in silica nanoparticles.[50] The processing parameters to note when making these nanocomposites are particle size (including average diameter and polydispersity), dispersion quality, and nanoparticle interface.

In this thesis, a novel family of two-dimensional transition metal carbides and nitrides, called MXenes have been used to synthesize epoxy nanocomposites.

1.2.4 MXenes

MXenes are a class of two-dimensional transition metal carbides, carbonitrides and nitrides that were first reported in 2011.[51,52] They possess the general formula $M_{n+1}X_nT_x$ (n=1-3) where M represents an early transition metal, X is carbon, nitrogen or both, and T_x denotes surface terminations such as hydroxyl, oxygen or fluorine.[53] They are formed by the selective etching of certain atomic layers from layered precursors such as MAX phases. MAX phases are a family of layered ternary carbides and nitrides that have the same $M_{n+1}AX_n$ formula, with the A element, representing a group 13 or 14 element, is interleaved between the $M_{n+1}X_n$ layers.[54] The M-A bond in MAX phases is more chemically reactive than the stronger M-X bond, and hence selective etching of the A-elemental layer is possible. $Ti_3C_2T_x$ was the first reported MXene, formed by the selective etching of the aluminum layer from its precursor Ti_3AlC_2 MAX phase.[51] More than 19 different MXenes have been synthesized thus far.[55-60] Dozens more are theoretically predicted.[61]

Various methods of synthesizing MXenes have been discovered, with MAX phases not the only precursors available for their synthesis. But MXenes, which have

been synthesized from MAX phases, can only be successfully etched when the MAX phases have Al as the A-element, even though more than 10 different Group 13 or 14 elements can be used to make MAX phases. Acidic aqueous fluoride-containing solutions have been used to etch the Al layer, such as aqueous hydrofluoric acid (HF)[53] or *in situ* HF formed through the reaction of hydrochloric acid and a fluoride salt[62]. MXenes have also been synthesized from non-MAX phase precursors. Examples are Mo_2CT_x which is synthesized by etching the Ga layers from Mo_2Ga_2C[60,63], and $Zr_3C_2T_x$ which is synthesized by selectively etching the aluminum carbide (Al_3C_3) layers from $Zr_3Al_3C_5$[64]. High temperature etching can also yield MXenes as was shown by etching the Al layer from Ti_4AlN_3.[59] All these etching methods do not create single flakes of the MXene, but rather stacked multilayered MXenes which then have to be delaminated into single flakes. In order to do this, first MXenes have to be intercalated by polar solvents, such as dimethyl sulfoxide (DMSO)[65,66], or large organic base molecules, such as tetrabutylammonium hydroxide (TBAOH)[67]. Intercalation of these molecules in MXenes has to be followed by mechanical vibration or sonication in water to yield colloidal solutions of single- or few-layer MXenes. In the case of the *in situ* HF synthesis route, colloidal solution of MXene flakes can be obtained by washing the reaction mixture till its pH reaches 6, without any additional step.[68] The acidic-fluoride containing solutions used to etch MXenes impart a mixture of –F, -OH and –O surface terminations, abbreviated by using T_x. The etching conditions and delamination steps that differ for MXenes, also impart different surface terminations.

MXenes possess both metallic conductivity of transition metal carbides and hydrophilicity as a result of their –OH or –O surface terminations. The wide variety of

transition metals that can be used to make MXenes shows the possibility of using them in applications ranging from electrochemical storage devices, such as battery electrodes[56,69,70] or electrochemical supercapacitors[55,62,71], to electromagnetic interference shielding devices[72]. Structural polymer composites[73,74], water purification[75-77], dye adsorption[78], and electrocatalysts[79,80] are some other applications for which MXenes have been investigated. In this thesis, the synthesis of MXene-epoxy nanocomposites has been studied.

1.2.5 Graphene-epoxy nanocomposites synthesis

The graphene-epoxy nanocomposites system is most similar to the MXene-epoxy system investigated in this thesis. They both consist of epoxy matrices reinforced with two-dimensional, layered nanoplatelet structures. The exciting properties of the graphene nanoplatelets have made them a promising filler material in epoxies, to enhance their thermal, electronic and mechanical properties.[81-85] The study of MXene nanocomposites is conducted in light of similar promising property improvements. In order to obtain the potential property enhancements effective dispersion is a necessary parameter.[86-88] Dispersion depends on both kinetics and thermodynamics. Thermodynamically, a good solvent for the filler ensures resistance to agglomeration and results in a good interface between the filler and polymer. Kinetically, processing methods such as sonication and shear mixing are required to deagglomerate the nanoplatelets and create a uniform distributed material. The problem of dispersion, in nanocomposites in general, is a practical concern, dependent on chemical and physical processing, processing time, and

polymer cure. Significant research has been done to explore processing methods, both chemical solvent selection and physical dispersion methods. Below are a variety of methods used to synthesize epoxy nanocomposites with graphene sheets or expanded graphite.

One of the most common methods of epoxy nanocomposite synthesis is *in situ* polymerization[86,87]. In this method, the material is chemically pre-treated in order to make it into a nanoparticle. Next, the nanoparticle is dispersed into volatile solvent by physical methods, followed by mixture with the epoxy monomer. The volatile solvent is then removed, and a hardener is added to cure the composite. Two primary methods of chemical pretreatment to make graphite sheets exist[88,89]: the reduction of graphite oxide (GO) which produces chemically altered single-layers of graphene[90-95], and acid intercalation followed by thermal shock which produces few-layered stacks of expanded graphite (EG)[96-104]. The chemically-modified graphene (GO) nanosheets are dispersed in volatile solvents that are miscible in epoxy, such as acetone, via physical processing methods. Meanwhile, the expanded graphite is either dispersed in acetone as well or sometimes directly into the epoxy resin[101], when making epoxy nanocomposites. Several design challenges are posed when using *in situ* polymerization to make nanocomposites. Particle suspension, agglomeration and sedimentation issues, solvent removal issues, and particle-polymer interface issues are all affected by the type of processing pathway used. Similar concerns are compounded by scalability, materials cost and volatiles management when thinking about commercial manufacturing. These problems complicate the design and extend the processing time associated with producing epoxy composites on an industrial scale.

Instead, an alternate synthesis approach to epoxy nanocomposites that is simpler and straightforward is to use room temperature ionic liquids (RTILs) as the solvent for dispersion and curing agent.[7,9] They have been shown to electrochemically exfoliate graphite in graphene sheets[105-107]. Cation-π stacking[108] and electrostatic shielding[109] between graphite and RTIL have been suggested as reasons for their favorable interaction. Epoxy nanocomposites of carbon nanotubes and graphite nanoplatelets have been produced by using EMIM-DCN as the dispersant.[12,13] Shear was applied to mix the epoxy, RTIL and nanofillers to produce epoxy nanocomposites with properties comparable to nanocomposites produced using *in situ* polymerization. Figure 1.4 shows the ease of processing composites using shear, without the need for solvent removal.

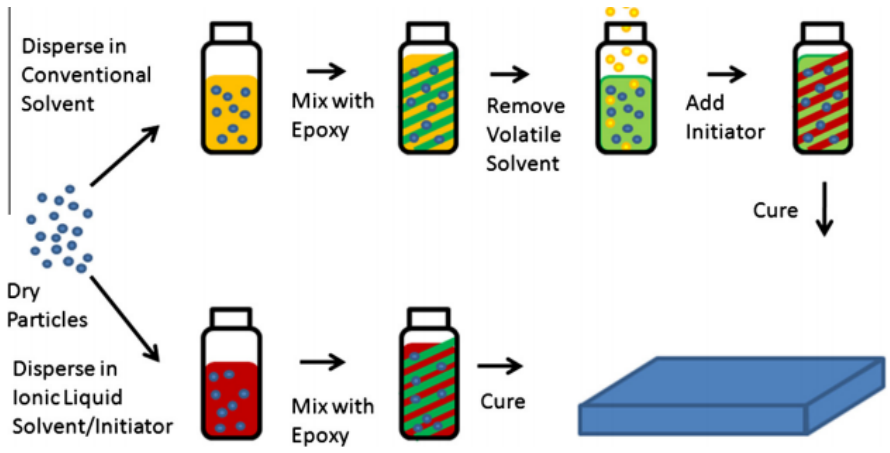

Figure 1.4: Schematic comparing in situ *polymerization involving a volatile solvent with epoxy nanocomposites processing using RTIL as a solvent and initiator. Adapted with permission from [12].*

An issue that needs to be highlighted when producing nanocomposites is that the interface between the filler and matrix is an important determinant of material properties.

The nanofillers have a high specific surface area, and hence the interfacial region becomes a dominant portion of the volume fraction of the matrix. The issues at the interface can be broken down into 3 factors, namely covalent bonding, wetting and particle clumping. A good interface features covalent bonding between the matrix and filler for optimum mechanical properties, as stress transfer can occur. But stress transfer can also occur without covalent bonding, as long as the wetting of the filler is sufficient. If wetting is poor, then the nanoplatelet acts as a void in the material, instead of as a reinforcement. Lastly, if particle clumping occurs when they are poorly dispersed, potential property enhancements will be hurt.

1.3 Overview

This thesis aims to show the success in using both *in situ* processes dependent on step growth polymerization, and laminar shear process that require chain extension polymerization to create MXene-epoxy nanocomposites.

Chapter 1 provides a background on epoxy chemistries, RTILs, MXenes, and nanocomposites and their synthesis. It introduces the motivation and approach taken to synthesize MXene-epoxy nanocomposites in this thesis. It also identifies parameters with which to judge the quality of composites synthesized.

In chapter 2, detailed descriptions of the synthesis techniques for making the MAX phases, MXenes and MXene-epoxy nanocomposites are given. Techniques used to characterize the nanocomposite are also discussed.

Chapter 3 provides results on Ti_3CNT_x-epoxy composites synthesized using the *in situ* polymerization method. The concerns regarding the method to make these nacre-like artificial structures, and the concerns regarding filler and epoxy interaction are detailed.

Chapter 4 examines the use of laminar shear stresses to exfoliate single layers from multilayered $Ti_3C_2T_x$ while dispersed in an epoxy and RTIL mixture. The effectiveness of producing good nanocomposites from this initiator-dispersant system are quantified, and the mechanisms of exfoliation and intercalation of the $Ti_3C_2T_x$ layers are explored.

Finally, chapter 5 offers a summary of the work carried out in this thesis. It also offers suggestions for future work to optimize the MXene-epoxy processing, and identifies other areas for exploration related to the chemistry of the MXenes.

Chapter 2: Materials and Methods

2.1 Synthesis of the MAX Phases

The MAX phases synthesized in this work are Ti_3AlC_2 and Ti_3AlCN. The Ti_3AlC_2 powder was synthesized by first mixing Ti_2AlC (>92wt.%, Kanthal, Sweden) and TiC (99%, Johnson Matthey Electronic, NY) in a 1:1 ratio, using zirconia balls in a plastic jar for 24 hours. The mixture was heated to 1350°C for 2 hours under argon, Ar, in a tuber furnace at a heating rate of 10°C/min. The Ti_3AlCN powder was produced by mixing titanium (99.5%, Alfa Aesar, Ward Hill, MA), AlN (99%, Sigma Aldrich, St. Louis, MO) and graphite (99%, Alfa Aesar, Ward Hill, MA) in a 3:1:1 ratio for 24 hours. The mixture was heated in a tube furnace under Ar at 1500°C for 2 hours, at a heating rate of 10°C/min. The MAX phases produced were furnace cooled to room temperature, and the resulting powder compact was milled using TiN coated drill bits to obtain powder. The Ti_3AlC_2 powder was sieved through a -200 mesh to obtain particles of size <35µm, while Ti_3AlCN was sieved through a -400 mesh to obtain <75µm powder.

2.2 Synthesis of MXenes

The exfoliation of the MAX phases to form their MXenes was carried out by using hydrofluoric acid (HF) (48-51%, Fisher Scientific, Fair Lawn, NJ). The sieved precursor powders were immersed in HF in a plastic container and stirred at 400RPM. The $Ti_3C_2T_x$ synthesis was carried out by using 10% HF at 35°C for 18 hours to etch its MAX phase. The Ti_3CNT_x synthesis was done by using 15% HF at 35°C for 18 hours to

etch the Ti_3AlCN phase. One gram of each MAX phases powder was added to 10 ml of the HF solutions used. After the specified etching time was completed, the contents of the reaction vessel were washed several times using deionized (DI) water and a centrifuge. The MXene particles sedimented after centrifuging at 3500 RPM for a few minutes, and the liquid was decanted and fresh DI water was added to disperse the sediment. This step was repeated until the decanting liquid had a pH of approximately 5. The sediment was dispersed in DI water once more, and filtered using a vacuum filtration setup, yielding multilayered MXene particles. The $Ti_3C_2T_x$ powder was used in its multilayered form in this thesis, and no delamination step was required.

Meanwhile, to produce delaminated flakes, the multilayered Ti_3CNT_x powder was added to tetrabutylammonium hydroxide (TBAOH) (40wt% in water, Sigma Aldrich, St. Louis, MO) in a ratio of 1gram powder to 10ml solvent and stirred for 2 hours. The mixture was centrifuged at 3500 RPM for 5 minutes, the supernatant was discarded, and the sediment was dispersed in 50 ml of DI water. This Ti_3CNT_x mixture in water was added to a 50ml glass vial, and sonicated using a probe sonicator at 1 hour, while a cooling system was used to cool the mixture to -10°C. After sonication, the solution was centrifuged for 1 hour at 3500 RPM, and the resulting black supernatant is a delaminated solution of Ti_3CNT_x in DI water. This dispersion was filtered into films by vacuum filtration, in order to be used in epoxy processing.

2.3 Epoxy Synthesis

The delaminated Ti_3CNT_x film was used to make epoxy nanocomposites using an *in situ* polymerization technique, while the $Ti_3C_2T_x$ powder underwent a laminar shear

processing regimen to create epoxy composites. DGEBA (Miller-Stephenson EPON 828, EEW 188gram/eq) was the epoxy monomer used in both techniques. The amine curing agent used was 4,4'-diaminodicyclohexylmethane (PACM curing agent, Air Products, AEW 52.5g/eq). EMIM-DCN (1-ethyl-3-methylimidazolium dicyanamide, >98.5%, Sigma Aldrich, St. Louis, MO) was the RTIL used.

2.3.1 In-situ polymerization

The filtered Ti_3CNT_x film was broken into smaller bits, and added to acetone in a 20ml glass vial. The mixture was bath sonicated for 5 hours. Once the Ti_3CNT_x dispersion in acetone was determined to be sufficient, an appropriate amount of DGEBA and PACM hardener were added to the acetone dispersion in the vial. This mixture was mixed in a Thinky rotational mixer for 10 minutes at 2000 RPM, and the vial was left out to dry in air at room temperature. This drying portion would allow the volatile solvent, acetone, to evaporate. Finally, the composite that had settled at the bottom of the vial was cured at 70°C for 4 hours and 160°C for at least 2 hours. Nacre-like composites were attempted to be synthesized via this method, and the MXene concentration varied between 10wt% to 90wt%.

2.3.2 RTIL polymerization

Multilayered $Ti_3C_2T_x$ MXene was used to make epoxy nanocomposites via a laminar shear processing regimen that involved EMIM-DCN as the RTIL dispersant and hardener. The MXene was first dried at 120°C under vacuum to remove water, as it may

hinder epoxy cure. The dried powder was mixed with epoxy and the ionic liquid (17.6 phr EMIM-DCN relative to EPON 828). The mixture was passed through a 3-roll mill (Torrey Hills T50), which had a 50mm roller diameter and roller speeds of 723, 394 and 219 RPM. The roller speeds correspond to surface velocities of 1.89, 1.03 and 0.573 m/s. The shear experienced by the mixture was controlled by adjusting the nip width (the gap) between the rollers and the viscosity of the mixture. The processing regimen involved a variable nip width schedule.

Table 2.1: Variable gap size of 3-roll mill used in the processing technique to make $Ti_3C_2T_x$-epoxy composites.

run number	nip width (µm)
1-4	80
5-12	24
13-22	6

These nip widths were used for both rollers. The roller gap size was controlled by using a spacer as the rollers were being brought together. A sheet of paper was the spacer for the largest gap size, Celgard was the spacer for the intermediate gap, and a Mylar® (BoPET) thin film used to cover x-ray fluorescence (XRF) sample cups was the spacer for the 6µm distance. After laminar shear processing, the mixture was degassed and thermally cured in molds at 80°C for 4 hours and 120°C for 3 hours. Epoxy nanocomposites were made with the $Ti_3C_2T_x$ filler concentration as high as 20wt.%.

A control sample was made with EPON 828 and PACM curing agent, which was first mixed in a rotational mixer, degassed and thermally cured at 80°C for 4 hours and

160°C for 2 hours. Some samples, which contained no RTIL, were also processed through the 3-roll mill. The processed epoxy mixture was then mixed with the PACM curing agent and cured in the same method as that used for the control.

2.4 Characterization Techniques

X-ray diffraction, XRD, patterns were obtained using Cu Kα radiation from a Rigaku SmartLab diffractometer (Tokyo, Japan). The step scans was set at 0.02° and 1s per step. Diffractograms of MXene powder particles were done by first pressing the powder by hand. The XRD of the epoxy nanocomposite parts was done on the polished side of a cured sample.

Low and high resolution micrographs were taken using transmission electron microscopy (TEM) (JEOL-2100, Japan) at an acceleration voltage of 200kV. Colloidal solution of MXene flakes were dropcast onto 200-mesh lacey carbon copper grids. Composite samples were mounted in epoxy and allowed to cure for 24 hours. Samples were then microtomed to obtain cross-sectional images of the sample structure.

Micromechanical properties of MXene-epoxy composite samples were measured using MTS Nano Indenter XP. Samples were mounted in an epoxy resin-hardner system for 24 hours. Mounted samples were then polished using silicon carbide grinding papers with increasing grit from 400, 800, then 1200. Samples were then polished further using 3, 1, then 0.5 micron polishing cloth with corresponding diamond suspension solution. Nanoindentation was performed using a 5 micron spherical tip with 15-20 locations taken per sample.

Chapter 3: In Situ Polymerization of MXene-Epoxy Nanocomposites

3.1 Design of Experiment

Nacre, otherwise known as mother of pearl, is a composite made up of a large quantity (up to 95wt.%) of platelet-like calcium carbonate ($CaCO_3$) filler.[110] An organic matrix exists between the fillers that maintains transverse integrity during slip, absorbs exceptionally high amounts of energy before failure, and exhibits crack deflection as a result of the high filler loading.[111,112] The enhanced mechanical properties, such as increased fracture toughness and tensile strength, exhibited by this naturally-occurring material are due to its highly regular microstructure, and good adhesion between the matrix and filler.[111] The potential property enhancements as a result of similar microstructures has led to increasing research on similar composites consisting of platelet-like fillers, such as $CaCO_3$ platelets, boron nitride and graphene oxide nanosheets, and a variety of polymers as the organic matrix.[113-115] In this thesis, epoxy nanocomposites with high quantities of Ti_3CNT_x were synthesized to obtain similar benefits.

3.2 *In situ* polymerization

The delaminated Ti_3CNT_x film was dispersed in acetone, a volatile solvent used most often for *in situ* polymerization of epoxy composites, because of its low boiling point. This MXene was selected in particular because it showed the most promise in being dispersed in acetone. $Ti_3C_2T_x$ dispersions in acetone only display short-term

stability, and begin to precipitate in a matter of days.[116] In order to produce nacre-like, MXene-epoxy composites, a large quantity of the nanofiller with respect to epoxy was needed, and that signals a requirement for a large quantity of MXene dispersed in acetone, which is not possible with $Ti_3C_2T_x$. The dispersions of Ti_3CNT_x in acetone remain more stable in comparison. Followed by their dispersion in acetone, the epoxy resin and amine hardener were added in small quantities, in appropriate ratios to the filler.

Even though research has shown promise in producing large scale delamination of Ti_3CNT_x[67], only small quantities of the delaminated MXene could be effectively produced in a lab setting, and this meant only small amounts of the organic matrix were added. The result was an epoxy nanocomposite that could not be poured into a mold, both because only small amounts of the composite could be made and because high loading of Ti_3CNT_x increased the viscosity substantially. Instead, the composites had to be cured in the glass vial. If the MXene loading was low enough, it would cure in the form of small cylindrical discs. But at higher loadings, as the acetone evaporated, the composite cured in small pieces. An interesting observation is the formation of jelly-like substance as acetone evaporates, eventually becoming solid when all the acetone has evaporated. Characterization of these Ti_3CNT_x-epoxy composites was carried out by breaking the discs into pieces, or using the pieces themselves. These pieces would be mounted in epoxy for nanoindentation and TEM imaging.

Figure 3.1(A) shows the load vs. displacement curves for Ti_3CNT_x-epoxy nanocomposites, and (B) shows the Young's modulus values of this system in comparison to other epoxy composites made with nanofillers. The load vs. displacement curves show that the load required to indent 2μm into the composites lies between that

required to indent the neat epoxy and pure delaminated Ti_3CNT_x film. In other words, there is no enhancement of mechanical properties of epoxy, beyond that of the filler, due to loading of the MXene via this *in situ* polymerization method. This fact is more apparent from the mediocre Young's modulus results. As filler loading increases, the modulus value only begins to approach the value for the delaminated Ti_3CNT_x film. No synergy between the matrix and the filler appears to exist, presumably as there is no covalent bonding between the filler and matrix exists, which prevents efficient stress transfer.

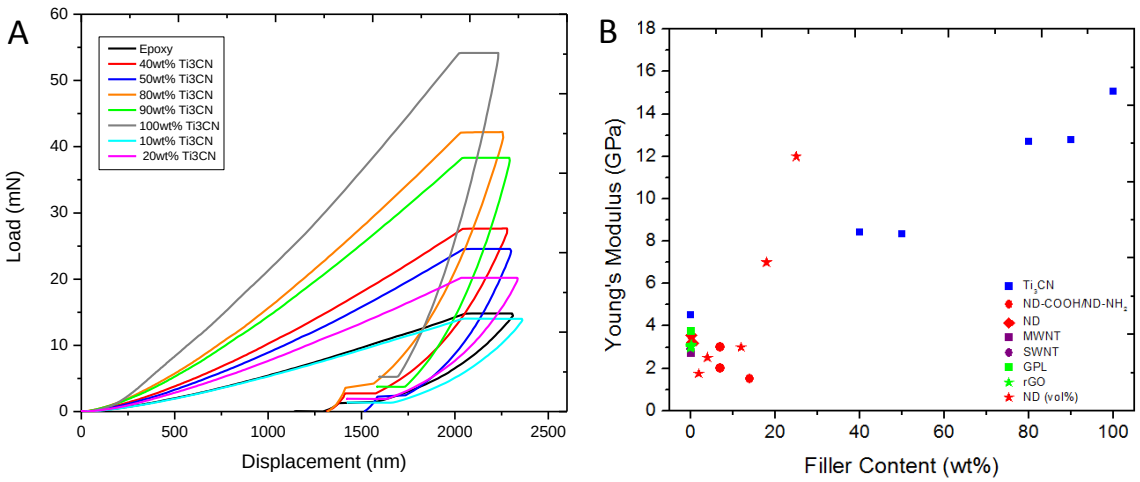

Figure 3.1: (A) Load vs. displacement curve obtained from nanoindentation for Ti_3CNT_x-epoxy composites, with different filler loadings. (B) Young's modulus for Ti_3CNT_x-epoxy, and other epoxy nanocomposites, as a function of filler content.

TEM images of the 50wt% composite, in Figure 3.2, shows that even though there are single layers of Ti_3CNT_x dispersed in the matrix, the more common feature is large Ti_3CNT_x particles that are still multilayered, seen in Figure 3.2(C-D). The processing

technique was not successful in completely exfoliating the multilayers into single layers of Ti_3CNT_x. This lack of dispersion of the MXene flakes is another reason for the poor mechanical performance observed from this composite. Combined with the lack of covalent bonding between the matrix and the filler, it is more likely that these Ti_3CNT_x clumps act similar to voids rather than as a reinforcement material.

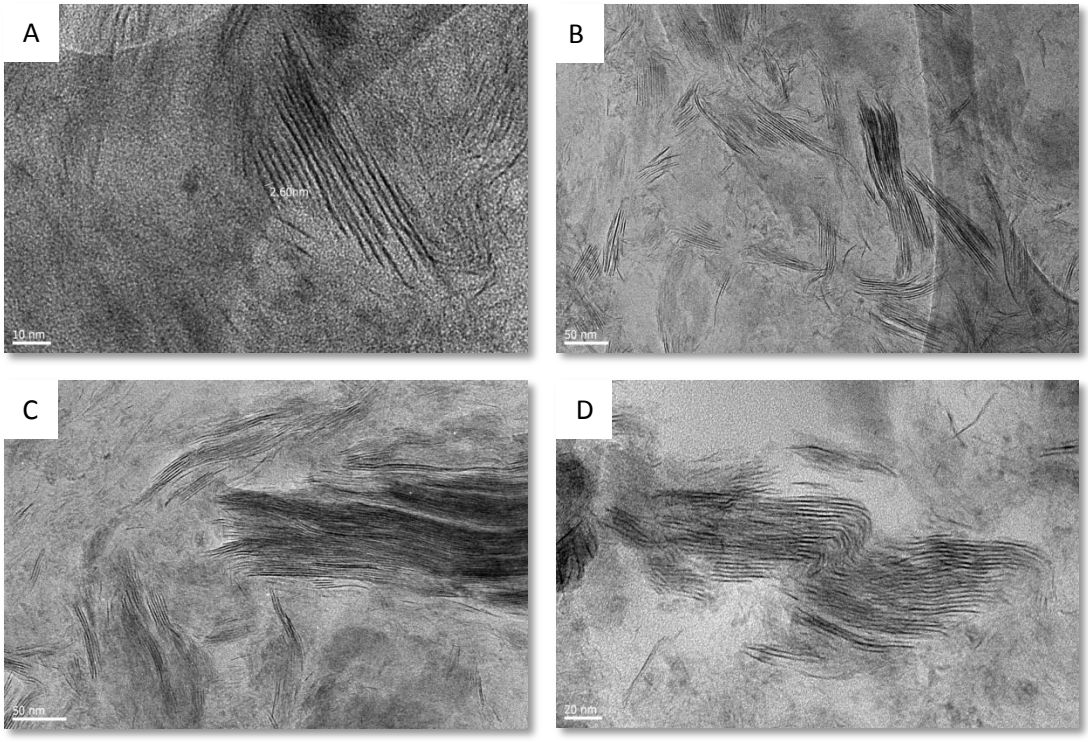

Figure 3.2: (A-D) TEM images of a 50wt% Ti_3CNT_x-epoxy composite, showing large Ti_3CNT_x particles that are not well dispersed or distributed through the matrix.

3.3 Conclusions

A combination of poor Ti_3CNT_x dispersion in epoxy, seen from TEM, and no covalent bonding between the epoxy matrix and filler is responsible for the lack of

mechanical property improvements. Moreover, since the filler is hydrophilic, it has poor wettability with the organic epoxy matrix, further hindering any potential stress transfer. As a result, the Ti_3CNT_x surface needs to be modified for better interaction with the epoxy matrix, in order to realize the potential property enhancements. It has to be noted that nanoindentation is unlikely to give a good representation of bulk properties of the material, due to the fact that the clumps of MXene that form are also on the same order of magnitude as the indent.

The major limitation of trying to create nacre-like composites using MXene, via this synthesis technique, is that it is a cumbersome process, with limited potential for scalability. The harsh, and long, sonication will create many defects in the MXene, lowering property enhancements. The inability to process composite parts of various shapes and sizes via this technique as a result of small yield and large viscosity also severely hampers potential applications. Nonetheless, this work has shown the potential to use *in situ* polymerization to create epoxy nanocomposites with MXenes, especially at lower filler loadings. It has also shown the need for study on engineering surface terminations and functionalizing the MXene surfaces, in order to create covalent bonding between the filler and the matrix.

Chapter 4: Direct Preparation of Few Layer MXene-Epoxy Nanocomposites from Multilayered MXene

4.1 Design of Experiment

The previous chapter has shown the need for simpler methods of producing epoxy composites with MXenes, in order to realize their full potential in a variety of applications requiring property enhancements, such as higher toughness, conductivity or electromagnetic interference shielding. Scalable approaches of dispersing single-layer flakes of MXene in matrices from their multilayered precursors, without the need for delamination steps, is therefore a high priority. Recent work has shown imidazolium-based room temperature ionic liquids (RTILs) are a unique system that offers opportunities for graphite exfoliation and dispersion[105-107], and also polymerization of epoxies[5]. This means the RTIL can serve as a solvent for the filler and hardener for the epoxy matrix, eliminating the need for solvent removal during processing.[12,13]

The ability for RTIL to disperse graphite provides a thermodynamically stable suspension, but kinetic forces are still necessary to overcome interlayer attraction, and exfoliate it into graphene. Some examples used of this kinetic treatment are sonication[117,118], grinding[119], twin-screw extrusion[120], and ball-milling[121,122]. Sonication results in extreme local conditions at the nanoparticle surface due to frequency-modulated compression/rarefication waves, that also feature violent cavitation and turbulent fluid flow.[123] The conditions include pressure up to 1000 bar, temperature up to 5000K, and cooling rates of more than 10K/s.[124] Sonication works by first peeling off the peripheral layers from stacked nanoparticles, and requires a great deal of time to exfoliate

internal layers.[117] Another method to shear the graphite layers, that is of special significance to this thesis, is the use of a 3-roll mill to provide laminar shear on the layers. It has been used in exfoliating graphite[14,125] and dispersing nanoparticles[97,126,127]. Instead of chemical processing, an approach combining RTIL as the solvent and initiator, and laminar shear for kinetic treatment was used to synthesize $Ti_3C_2T_x$-epoxy composites. This same approach was used to synthesize graphene-epoxy composites from untreated graphite.[14] Multilayered $Ti_3C_2T_x$ MXene was mixed with EPON 828 and 1-ethyl-3-methyl imidazolium dicyanamide (EMIM-DCN). The mixture was processed through the 3-roll mill to apply shear stress on MXene particles to exfoliate them, with the RTIL expected to minimize agglomeration or restacking of the flakes and to induce cure. And since RTIL is a latent initiator, leaving the mixture over months would not solidify it.

The schematic in Figure 4.1 shows the path of the $Ti_3C_2T_x$- epoxy mixture through the 3-roll mill. The three rolls are the feed roll, center roll and apron roll, noted in the schematic as Fig. 4.1(B, C, F), respectively. The speed of the rolls increases at a ratio of 1:1.8:3.3, with the speed of the rolls set at 219, 394, and 723 RPM, respectively. This corresponds to velocities of 0.573, 1.03, and 1.89 m/s. The material starts from the feed region between the feed and center rolls, before moving towards the gap between the center and apron rolls, and either recirculates back to the feed region or is collected off the apron.In a 3-roll mill, the maximum shear stress occurs at the nip, the region between adjacent rollers. A tradeoff occurs between having a large nip width for high throughput, and a small nip width for high applied shear stress. A variable nip width processing regimen in which the nip width narrows successively, and shear increases, is used. The

MXene-epoxy-RTIL mixture passed through the mill 22 times: 4 passes at 80µm roller gap, 8 passes at 24µm gap and finally 10 passes at 6µm gap.

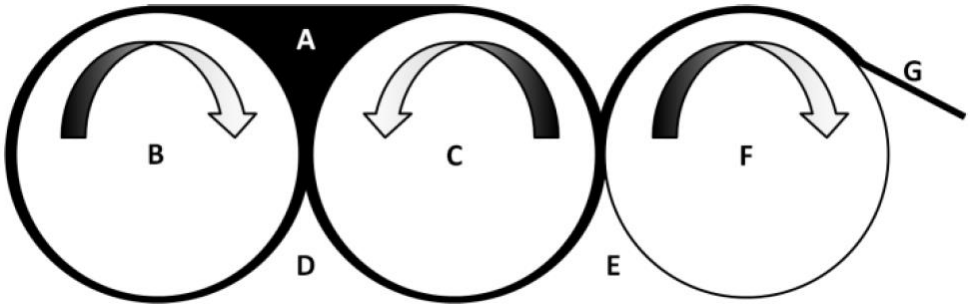

Figure 4.1: A schematic showing how a 3-roll mill functions. Adapted with permission from [14]. The sample is poured into the feed region (A) between the feed (B) and center (C) roll. As a result of the gap size, only some of the material passes through the first nip (D), with most of it remaining in the feed region. The material then flows through the second nip (E) between the center and apron (F) rolls. Here the material is either collected by an apron (G), or is recirculated into the feed region.

4.2 Theory

In a 3-roll mill, the velocity differential between adjacent rolls applies shear stress on the material flowing between it. The standard equation for Couette flow can be used to calculate shear stresses experienced by the material, assuming static, isobaric and laminar flow between parallel plates. According to this equation, the fluid shear stresses (τ) is a function of material viscosity (μ), roller velocities (u_1 and u_2), and nip width (L). The Couette flow equation is:

$$\boldsymbol{\tau = \frac{\mu * (u_1 - u_2)}{L}}$$

The value from this is the approximate shear stress, and can be compared with the interlayer coupling energies between adjacent layers of the multilayered $Ti_3C_2T_x$. Simulations have suggested that the primary mode that holds the this MXene in its stacked conformation is a combination of intermolecular interactions and hydrogen bonding.[128] The binding energies of the multilayered $Ti_3C_2T_x$ is expected to be 2 to 6 times stronger than that of graphite and MoS_2, both of which have weak interlayer coupling in the form of van der Waals interaction. The interlayer shear stresses (ISS) of graphite have been experimentally shown to range from 0.5[129] to 140[130] MPa. The lower values are due to variations in layer interactions resulting from deviations from the ideal AB stacking. Weaker graphite layers in the crystal were being sheared at the low shear stresses. Throckmorton et al. demonstrated delamination of graphene layers using laminar shear stress achieved by processing an RTIL-epoxy-graphite mixture through a 3-roll mill, which achieved approximate shear stresses of more than 140 MPa.[14]

In comparison to graphite, theoretical calculations suggest that $Ti_3C_2T_x$ has ISS around 280-840 MPa, with the variations resulting from different surface terminations. Bare nanosheets are expected to have stronger binding energies, while –F and –O terminated $Ti_3C_2T_x$ nanosheets produce lower ISS values.[128] The synthesis technique used does not provide control over the final surface terminations, but a random combination of -O, -F and -OH surface terminations are expected. In order to maximize shear according to the Couette flow equation, high roller velocities, low nip widths, and high MXene loadings are used to delaminate $Ti_3C_2T_x$ *in situ*. For this study the MXene loading used was as high as 20wt.%, to increase viscosity. Even though such high filler loadings are made, the final part need not contain such a high percentage of $Ti_3C_2T_x$, and

rather it can be diluted by the addition of the other components of the composite to obtain the desired ratio. X-ray diffraction (XRD) and transmission electron microscopy (TEM) were conducted on the final, cured epoxy composites to study the nature of the $Ti_3C_2T_x$ dispersion. Moreover, viscosity measurements were carried out to determine approximate shear stresses achieved via the processing regimen.

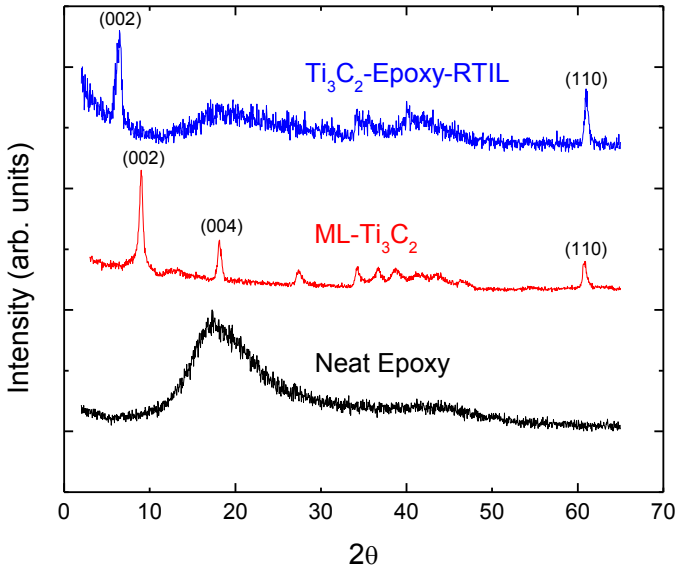

Figure 4.2: XRD patterns for neat epoxy, multilayered $Ti_3C_2T_x$ dried at 120°C, and a cured 10wt.% $Ti_3C_2T_x$-epoxy-RTIL composite.

4.3 Shear Processing

Figure 4.2 shows XRD patterns of the neat epoxy, dried multilayered $Ti_3C_2T_x$, and cured composite sample containing 10wt.% $Ti_3C_2T_x$. The epoxy has a broad peak around $2\theta = 17°$, while the MXene powder had distinct (002), (004) and (110) peaks at about $2\theta = 9°, 18°$ and $61°$, respectively. The d-spacing is the distance between adjacent planes in the material, which means the (002) peak corresponds to the distance between

two adjacent $Ti_3C_2T_x$ layers. The (110) peak is a result of ordering in the non-basal directions. Other peaks are present, are commonly observed in multilayered MXenes, and are not indexed here. After processing of the composite mixture through the 3-roll mill, and its curing, the (002) peak shifted from approximately $2\theta = 9°$ to $2\theta = 6.55°$, but the (110) peak was still present. When delamination of MXenes occurs into their single layers, the (110) peak disappears, or at least decreases substantially, as there is no longer any non-basal ordering. After 3-roll mill processing, the presence of the (110) peak means that single layers of $Ti_3C_2T_x$ were not successfully exfoliated. Instead, the d-spacing had increased from about 9.8 Å to approximately 13.5 Å. The $Ti_3C_2T_x$ multilayers had swelled after 3-roll mill processing.

Figure 4.3(A) depicts XRD patterns for other $Ti_3C_2T_x$ loadings produced via the same method, using both epoxy resin and RTIL. Even at a higher loading fraction of 20wt.%, the nanocomposite still had the (110) peak and also a similar (002) peak shift. The 1wt.% composite sample did not give any discernible (002) or (110) peaks, most likely because the $Ti_3C_2T_x$ loading was not sufficient to yield any signal. It can be theorized that delamination occurred as no $Ti_3C_2T_x$ peaks are observed, but conductivity measurements of the sample gave no value. At 1wt.% $Ti_3C_2T_x$, some conductivity increases are expected, but since none were observed it signals that delamination of the $Ti_3C_2T_x$ did not occur. Figure 4.3(B) zooms in on the (002) peak of the 10 and 20wt.% composites. The 20wt.% $Ti_3C_2T_x$ sample has 2 distinct peaks at $2\theta = 6°$ and 6.5° of equal intensity, while the 10wt.% has a much stronger peak at $2\theta = 6.5°$. An increase of about 4-4.5Å has occurred between adjacent $Ti_3C_2T_x$ layers in the composites, even as the multilayered structure remains.

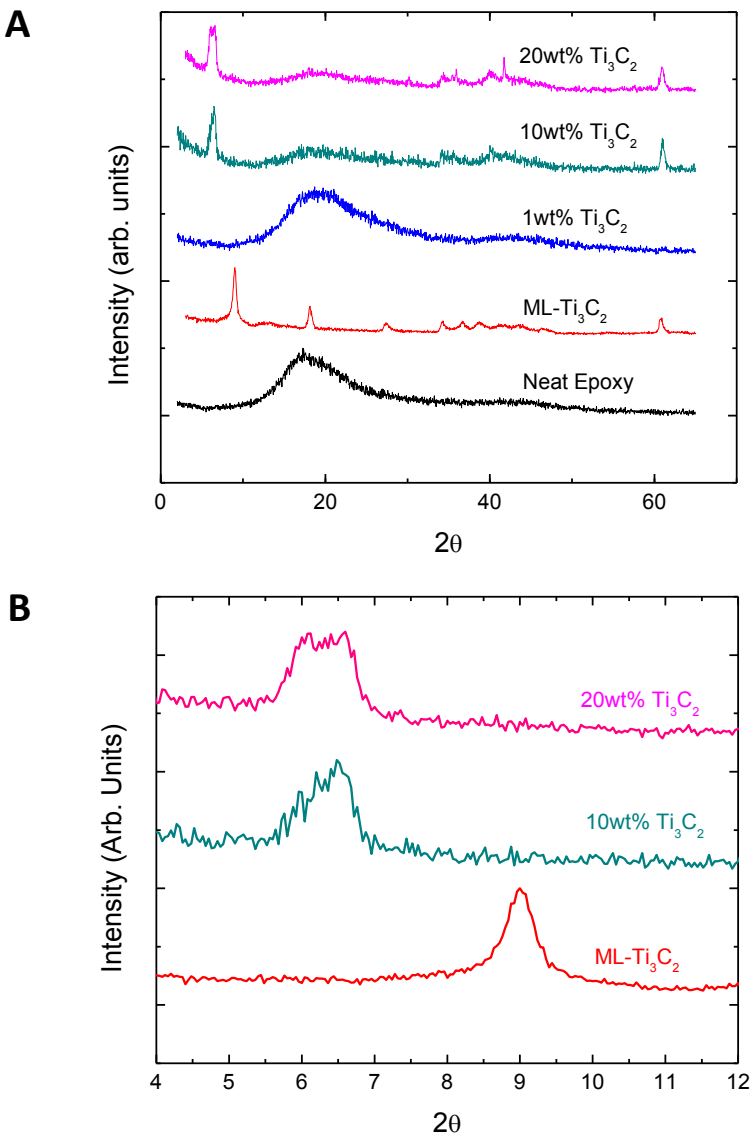

Figure 4.3: (A) XRD patterns for cured 1, 10 and 20wt% $Ti_3C_2T_x$-epoxy-RTIL composites, along with neat epoxy and pure MXene. (B) XRD pattern of multilayered $Ti_3C_2T_x$ dried at 120°C, and cured 10 and 20wt.% $Ti_3C_2T_x$-epoxy-RTIL composite, focusing on their (002) peaks.

Figure 4.4 and 4.5 show TEM images obtained for 10 and 20wt.% $Ti_3C_2T_x$-epoxy composites, respectively. The images further show that multilayered MXene particles are suspended in the matrix. Starting from MAX phase particles that are less than 75µm in size, to eventually ending with $Ti_3C_2T_x$ particles consisting of about 5-20 layers in the

composites, shows that the HF acid etching and 3-roll mill processing significantly decreased particle size. But exfoliation of single flakes was not achieved via this synthesis technique. TEM also shows that intercalation of the $Ti_3C_2T_x$ layers has taken place. But single layers of the $Ti_3C_2T_x$ filler were not observed suspended in the matrix. This is in good agreement with results from XRD.

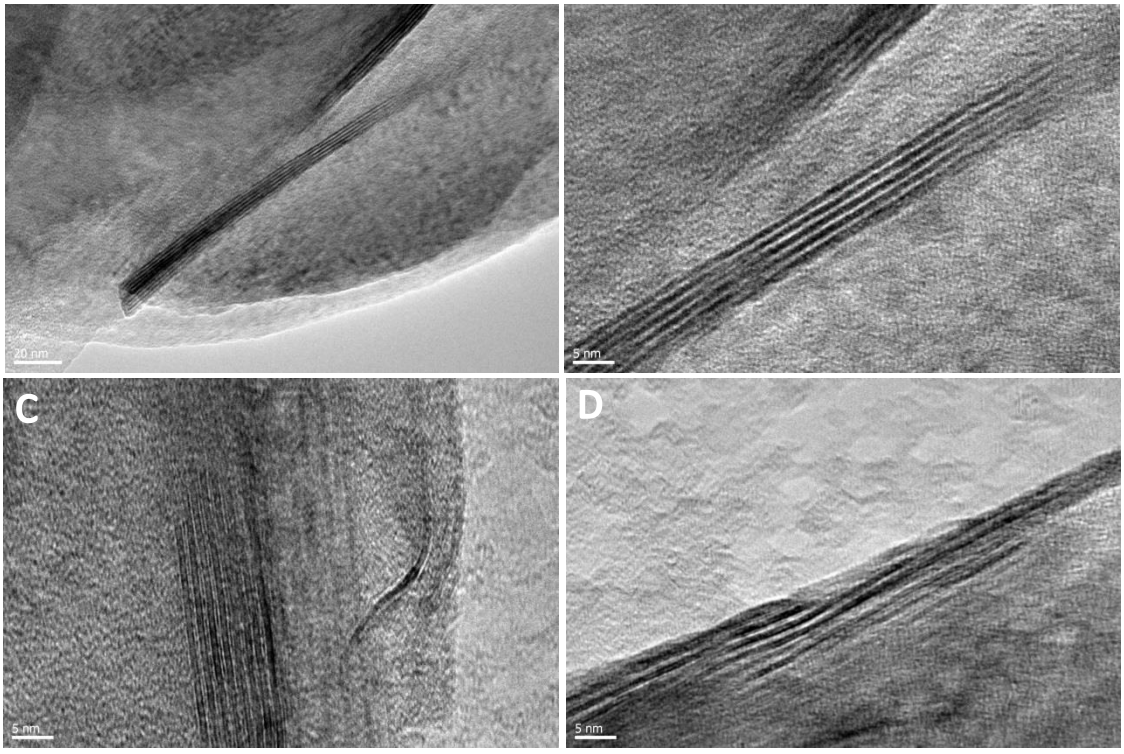

Figure 4.4: (A-D) TEM images obtained for a 10wt.% $Ti_3C_2T_x$-epoxy-RTIL composite.

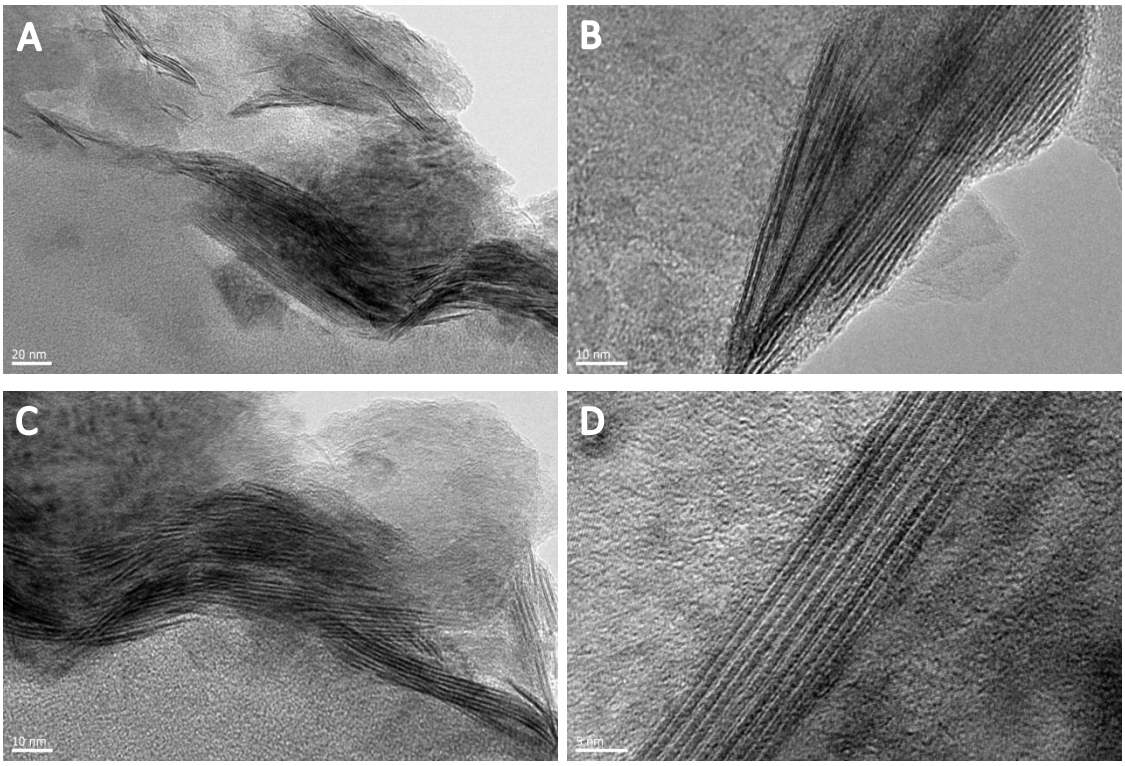

Figure 4.5: (A-D) TEM images obtained for a 20wt.% $Ti_3C_2T_x$-epoxy-RTIL composite.

In order to understand why delamination of the $Ti_3C_2T_x$ single layers did not occur, viscosity readings of the $Ti_3C_2T_x$-epoxy-RTIL mixture were taken before curing. Figure 4.6 shows the viscosity readings of the 1 and 20wt.% $Ti_3C_2T_x$-epoxy-RTIL mixture after passing through the 3-roll mill. Addition of 1wt.% of the filler results in a decrease in viscosity, but as filler content increases to 20wt.%, the viscosity increases. The viscosity of the epoxy-RTIL and the composites mixture does not show a strong trend as a function of shear rate, with the 20wt.% mixture showing signs of shear thinning behavior. Colloidal suspensions with high aspect ratio particles show a strong shear thinning effect, with viscosity decreasing drastically with increasing shear rate, because of the alignment of the particles in the direction of flow.[131] Similarly, if $Ti_3C_2T_x$

single layer flakes were suspended in the matrix, a strong shear thinning effect should have been observed for the mixture after 3-roll mill processing.

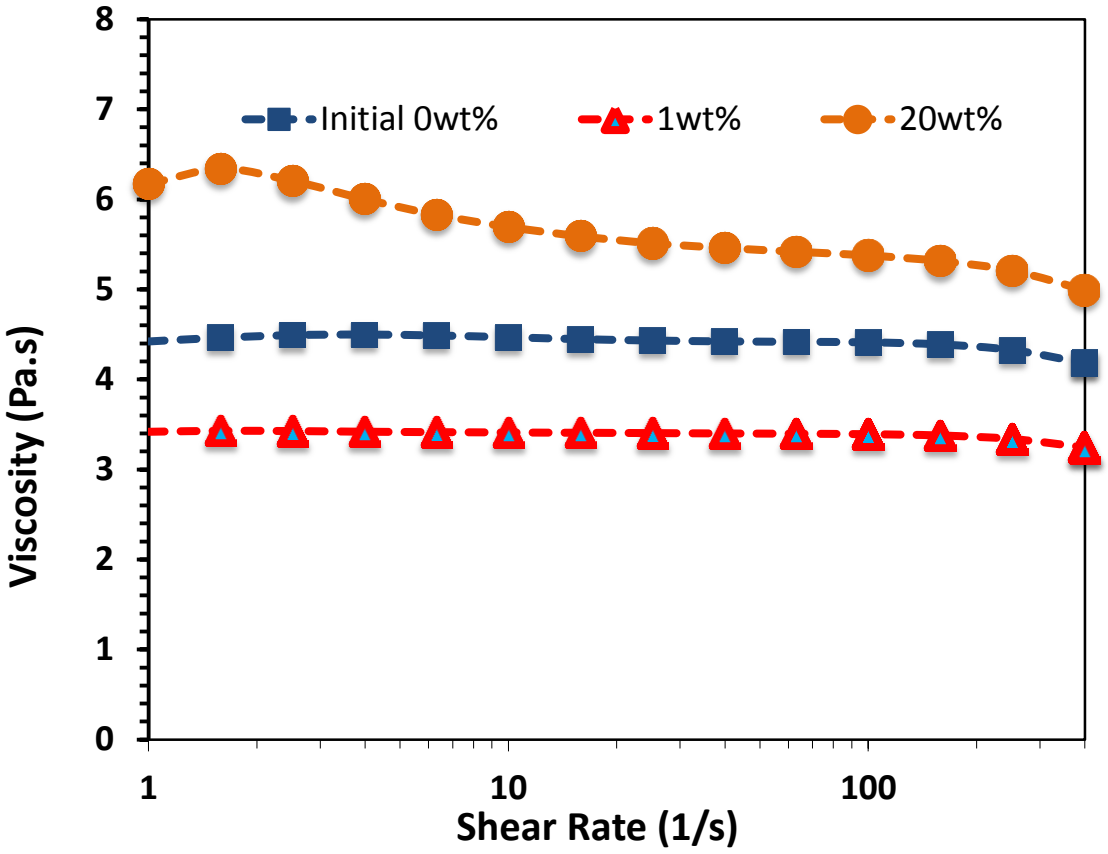

Figure 4.6: Viscosity readings of EPON 828 and EMIM-DCN mixture, and of 1 and 20wt.% $Ti_3C_2T_x$-epoxy-RTIL mixture after 3-roll mill processing are seen as a function of shear rate.

Using the viscosity readings taken at 25°C, the approximate shear stress on the $Ti_3C_2T_x$ particles in the mixture during 3-roll mill processing was calculated. Figure 4.7 shows the shear stresses experienced by a pure epoxy-RTIL and a 20wt.% $Ti_3C_2T_x$-epoxy-RTIL mixture. Passing through a nip width of 6µm, the pure mixture experiences

630 MPa of shear stress, while the $Ti_3C_2T_x$ particles in the 20wt.% composite experience about 860 MPa of shear. The calculated shear stresses are an approximate value, as the mixture viscosity decreases with increasing shear rate, a fact not taken into consideration. Hence, the applied shear stresses were lower than calculated. Even then, at shear stresses greater than 500MPa, some $Ti_3C_2T_x$ exfoliation was expected. The fact that this was not observed suggests the shear stress needs to be increased. This was achieved by processing $Ti_3C_2T_x$ composites through the 3-roll mill without any RTIL, and curing the mixture using PACM hardener.

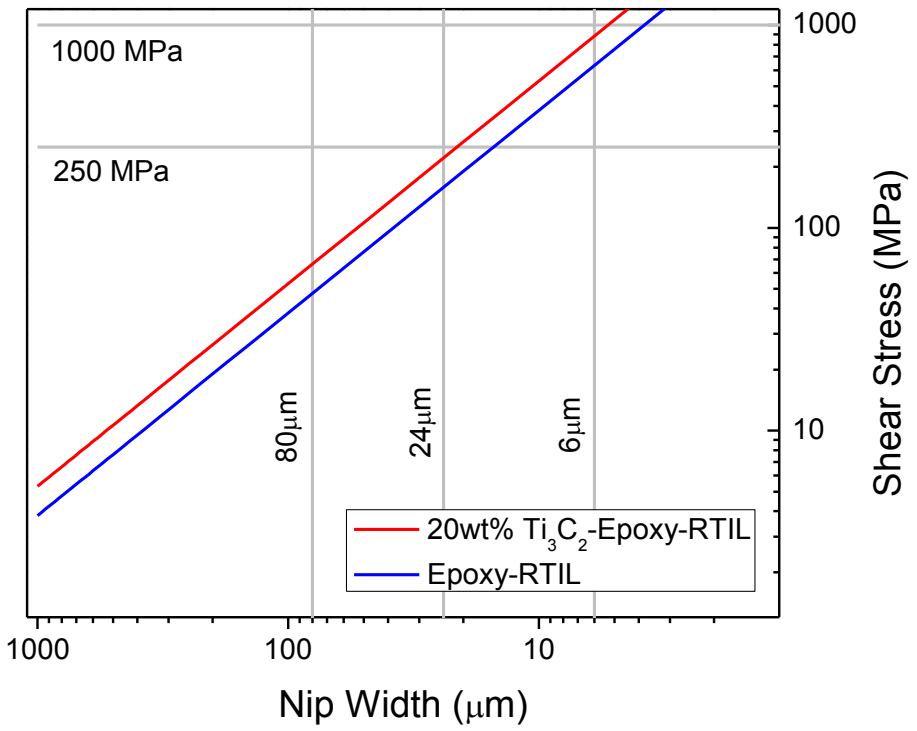

Figure 4.7: Approximate applied shear stress experienced by an epoxy-RTIL mixture, and by $Ti_3C_2T_x$ particles suspended in a 20wt.% $Ti_3C_2T_x$-epoxy-RTIL composite.

Figure 4.8 depicts XRD patterns obtained for 5 and 20wt.% $Ti_3C_2T_x$-epoxy nanocomposites which were processed through the 3-roll mill without the use of RTIL. The (002) peak is still visible for both composites at the same 2θ as that of the multilayer $Ti_3C_2T_x$. The signal for the 5wt.% composite is weaker, and hence the (002) and (110) peaks appear absent, but they are in fact still present at the same 2θ as $Ti_3C_2T_x$. The presence of the (002) and (110) peaks is more clearly observed for the 20wt.% specimen. This synthesis technique, which involved no RTIL, showed no interaction between the epoxy matrix and the $Ti_3C_2T_x$ filler. The $Ti_3C_2T_x$ particles appear to still be in their multilayer state after processing.

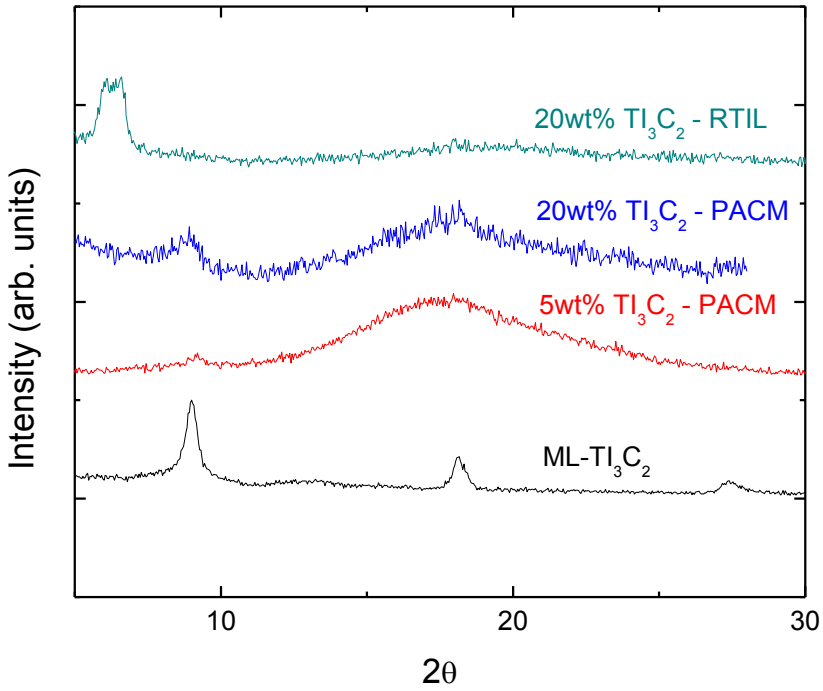

Figure 4.8: XRD patterns for $Ti_3C_2T_x$ composites processed through the 3-roll mill without any RTIL, and cured with PACM hardener.

Figure 4.9 demonstrates the viscosity of mixtures produced using the original and modified method. EPON 828 has a viscosity at 25°C of more than 10 Pa·s. If 20wt.% $Ti_3C_2T_x$ is mixed only with the epoxy resin for processing, its viscosity increases by a factor of 30. If RTIL is added to this mixture, the viscosity becomes lower by a factor of 50, around 6Pa·s. Both the 20wt.% $Ti_3C_2T_x$-epoxy mixtures with and without RTIL demonstrate some shear thinning behavior, but that behavior is not pronounced, suggesting single layers of $Ti_3C_2T_x$ were not successfully exfoliated.

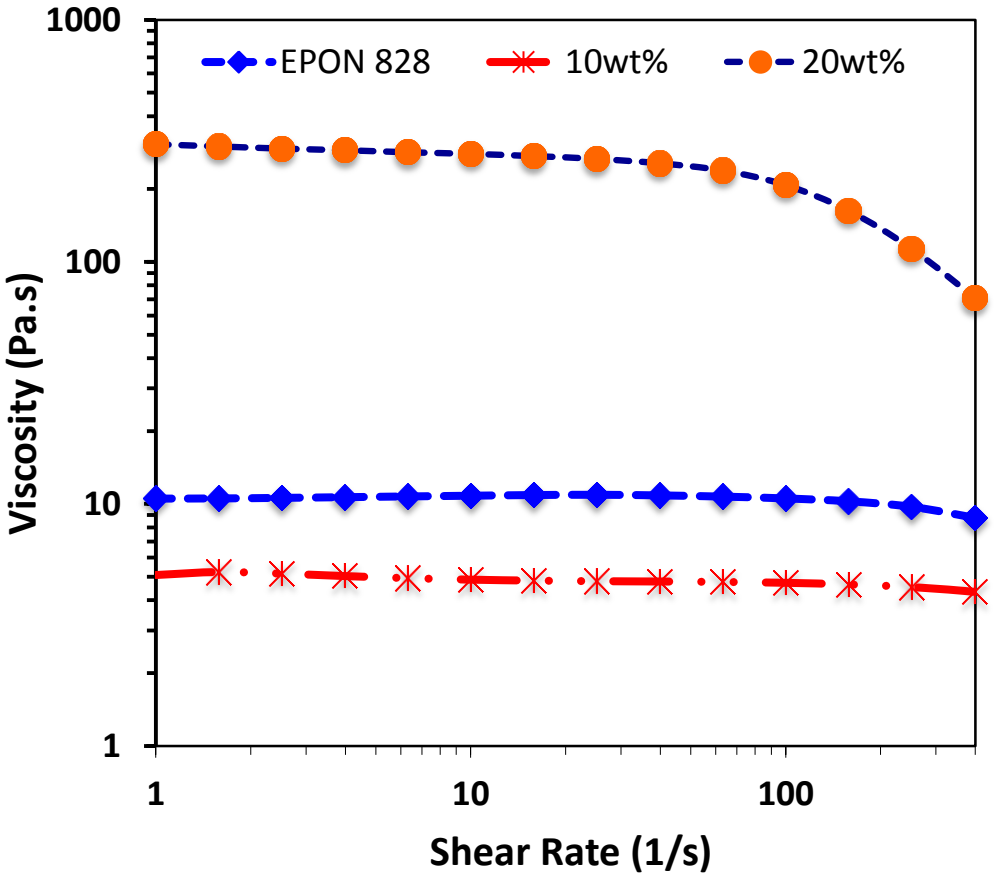

Figure 4.9: Approximate applied shear stress experienced by EPON 828, $Ti_3C_2T_x$ particles suspended in a 10wt.% $Ti_3C_2T_x$-epoxy-RTIL composite, and $Ti_3C_2T_x$ particles suspended in a 20wt.% $Ti_3C_2T_x$-epoxy composite, during 3-roll mill processing.

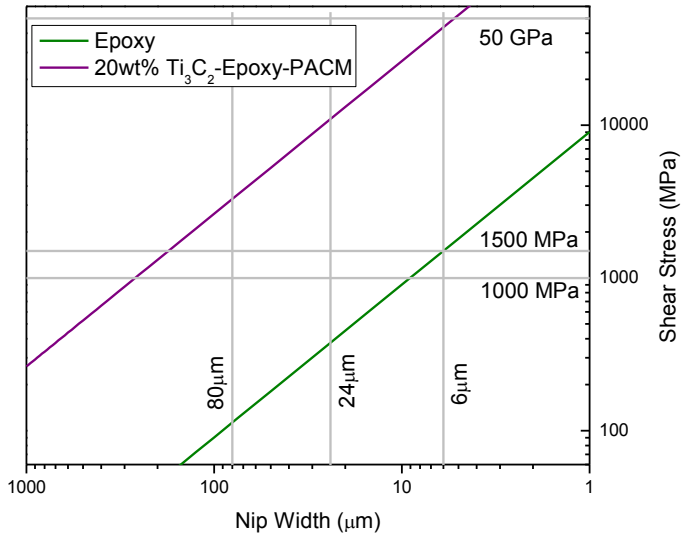

Figure 4.10: Approximate applied shear stress experienced by the pure EPON 828 resin, and by $Ti_3C_2T_x$ particles suspended in a 20wt.% $Ti_3C_2T_x$-epoxy only mixture.

Figure 4.10 shows the approximate values for laminar shear stresses on the $Ti_3C_2T_x$ particles suspended in a 20wt.% $Ti_3C_2T_x$-epoxy mixture. At the lowest gap size between the rollers, the shear stress value is calculated to be about 49 GPa, in comparison to laminar shear around 1.5 GPa for the pure epoxy resin, were it to be processed through the 3-roll mill. The $Ti_3C_2T_x$-epoxy mixture experiences shear stresses that are about 50 times that of the $Ti_3C_2T_x$-epoxy-RTIL mixture, at the same $Ti_3C_2T_x$ loading. It has to be stated that a shear value of 50GPa is meaningless, as the assumptions taken into account probably account for such a high value. Even then, the shear stresses are more than sufficient in theory to exfoliate single layers of $Ti_3C_2T_x$ via the 3-roll mill processing regimen. The XRD patterns still show all the $Ti_3C_2T_x$ peaks suggesting no exfoliation. This means that the shear stress was not transferred to the MXene particles, as at shear stress that is more than theoretically predicted interlayer coupling, should exfoliate

layers. Hence, shear stress transfer efficiency needs to be increased to produce optimum composites.

TEM images of the 20wt.% $Ti_3C_2T_x$-epoxy composites are shown in Figure 4.11. The $Ti_3C_2T_x$ layers have a well ordered structure in this composite, with no interruption of the stacking. The appearance of the $Ti_3C_2T_x$ layers in this composite are in contrast to TEM images of composites processed with RTIL, as it is apparent that no intercalation has taken place as well. It is hypothesized that no interaction between $Ti_3C_2T_x$ and epoxy exists, and hence processing through the 3-roll mill produces no discernible impact on the stacking of $Ti_3C_2T_x$. The addition of RTIL to the composites induces interactions between the filler and matrix upon cure, resulting in the increase in d-spacing.

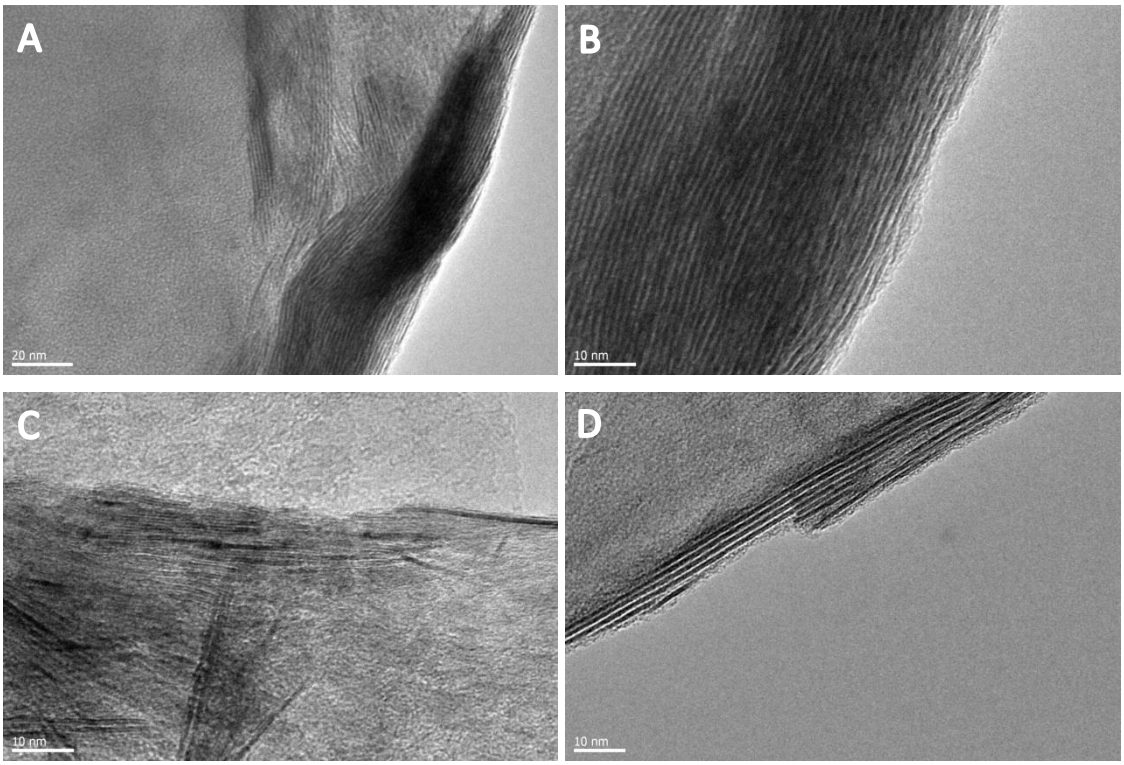

Figure 4.11: Approximate applied shear stress experienced by the pure EPON 828 resin, and by $Ti_3C_2T_x$ particles suspended in a 20wt.% $Ti_3C_2T_x$-epoxy only mixture.

Considering that the addition of RTIL to the $Ti_3C_2T_x$-epoxy system causes swelling of the $Ti_3C_2T_x$ layers, as a result of some intercalation reaction, a $Ti_3C_2T_x$-epoxy-RTIL specimen was made without any 3-roll mill processing. The mixture was put in a rotational mixer for 15 minutes at 2000RPM, and cured. Figure 4.12 gives the XRD pattern for this sample. This composite, like other composites made with RTIL, showed a shift of the (002) peak, indicating intercalation between $Ti_3C_2T_x$ layers. The inset shows that in the specimen with no 3-roll milling, the (002) peak at $2\theta = 6.5°$ is stronger than that at 6°, similar to the 10wt.% $Ti_3C_2T_x$-epoxy-RTIL specimen. The 20wt.% $Ti_3C_2T_x$-epoxy-RTIL sample meanwhile had similar intensities for both the (002) peaks.

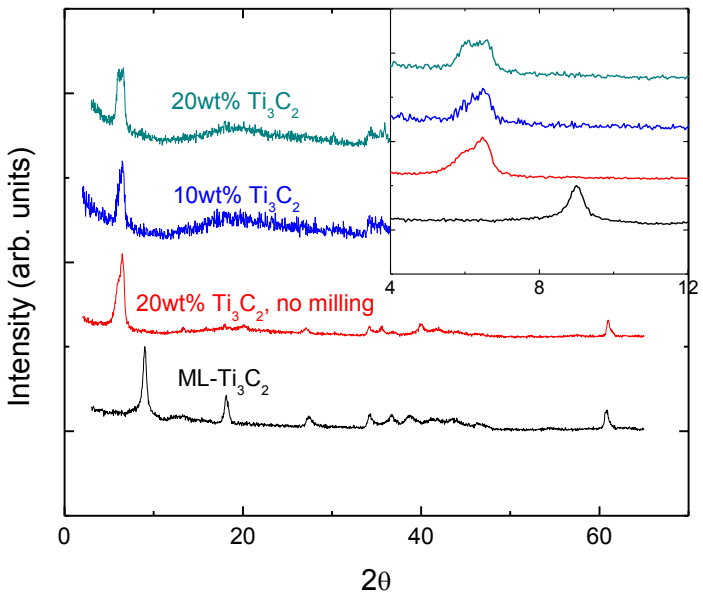

Figure 4.12: XRD patterns of $Ti_3C_2T_x$ multilayer, 10 and 20wt.% $Ti_3C_2T_x$ after 3-roll mill processing, and 20wt.% $Ti_3C_2T_x$ with no post processing. Inset shows details of (002) peak.

Figure 4.13 shows the XRD pattern obtained for $Ti_3C_2T_x$ powder that was mixed with the RTIL for 30 minutes, and then filtered. It shows the same peak shift to $2\theta =$

6.5°, which corresponds to an increase of about 4 Å. The interaction of an imidazolium-based room temperature ionic liquid, that is the same cation as the one used in this study, resulted in a similar peak shift in an earlier study.[132] In that study, the intercalation of the EMIM-based ionic liquid that resulted in d_{002} spacing increase of more than 4 Å, was linked to cation intercalation, as the cation had a size of around 4.4 Å. A similar observation in this work suggests a similar reason for the intercalation behavior observed, even though the anion in the RTIL used is different. The interaction between $Ti_3C_2T_x$ and RTIL then corresponds to the observed (002) peak shift from around $2\theta = 10°$ to 6.5°.

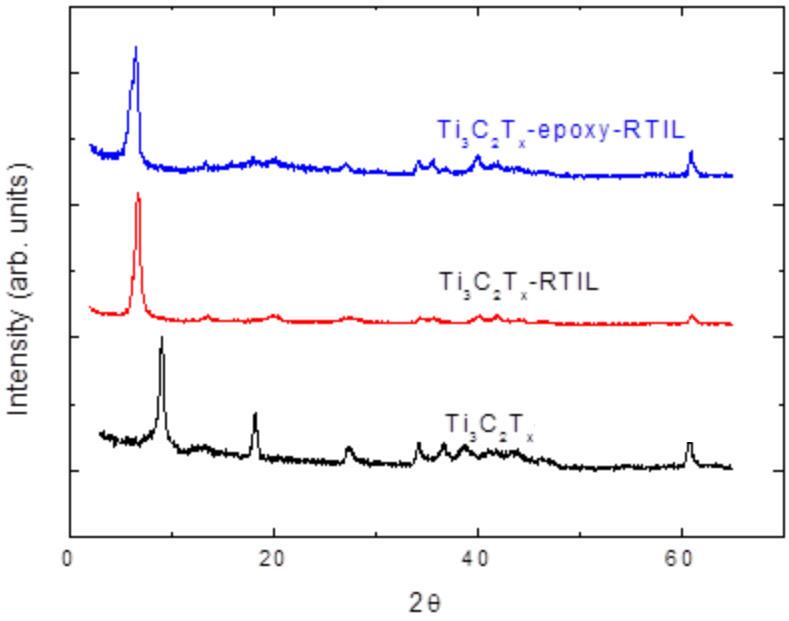

Figure 4.13: XRD patterns of multilayered $Ti_3C_2T_x$, $Ti_3C_2T_x$ powder mixed with the RTIL, and a cured $Ti_3C_2T_x$-epoxy-RTIL composite made with not 3-roll mill processing.

The ionic liquid dispersant/hardener induces intercalation of the between the $Ti_3C_2T_x$ layers in the composites regardless of processing method. But the reason for the

other (002) peak shift, that is to $2\theta = 6°$, is still not known. This higher d-spacing may correspond to epoxy intercalation, and not only RTIL intercalation. It was only observed only for the 20wt% $Ti_3C_2T_x$-epoxy-RTIL sample, and not even the 10wt% sample, after 3-roll mill processing. This means shear stress still plays a part in enhanced $Ti_3C_2T_x$ intercalation, as the shear stress on the former is greater than on the latter, owing to a higher viscosity from a higher $Ti_3C_2T_x$ loading.

The next step pursued was to enhance shear stress transfer in RTIL containing composites, in order to take advantage of the RTIL intercalation that allows for the potential intercalation of epoxy. Both the RTIL and DGEBA monomers are small, and hence are unable to transfer the shear stress to the $Ti_3C_2T_x$ particles effectively. In response, the mixture of $Ti_3C_2T_x$-epoxy-RTIL was first cured at 100°C for 30 minutes and then quenched, before processing through the 3-roll mill. The RTIL is a latent curing agent, and so only at this higher temperature, some opening of the oxirane ring occurs, leading to chain extension, and leading to some crosslink formation as well. This step is referred to as pre-curing, and samples made using this method are referred to as pre-cured $Ti_3C_2T_x$-epoxy-RTIL composites. The idea behind pre-curing the mixture is that the chain extension of the epoxy results in better shear stress transfer, and more $Ti_3C_2T_x$ cleavage, when processed through the 3-roll mill. The mixture is then cured like other RTIL composites.

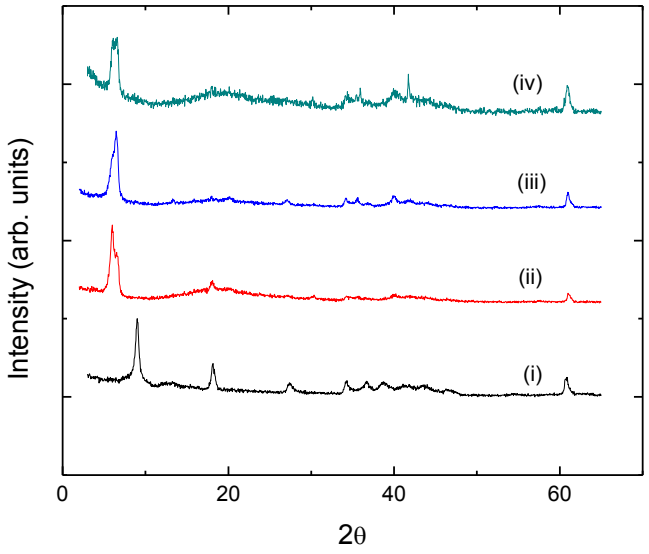

Figure 4.14: XRD patterns of (i) multilayered $Ti_3C_2T_x$, (ii) composite made with 20wt.% $Ti_3C_2T_x$ dispersed in pre-cured epoxy-RTIL mixture, (iii) 20wt.% $Ti_3C_2T_x$-epoxy-RTIL composite made using rotational mixer, and (iv) 20wt.% $Ti_3C_2T_x$-epoxy-RTIL composite made using 3-roll mill.

Figure 4.14 illustrates the XRD pattern obtained for a pre-cured 20wt.% $Ti_3C_2T_x$-epoxy-RTIL sample, in comparison to the XRD patterns of other RTIL composites. Figure 4.15 zooms in on the (002) peaks for these composites. An increase in the d-spacing of the $Ti_3C_2T_x$ is apparent, but what is more interesting is that the (002) peak at $2\theta = 6.5°$ is very small in comparison to the $2\theta = 6°$ peak. A majority of the $Ti_3C_2T_x$ particles are not only intercalated by RTIL, but also by something else that results in a d-spacing increase of about 5 Å. We hypothesize this may be a result of epoxy intercalation as well, but this assertion is not certain and needs to be tested. One observation in support of this hypothesis is that the pre-cured composite is the only composite in this whole thesis which yielded a conductivity value, of about $1 \times 10^{-4} S/m$. This value is not great, but is a step in the right direction, as all the other composites gave no readings. The observation of some conductivity may demonstrate the beginnings of the formation of a percolating network, suggesting delamination of multilayered $Ti_3C_2T_x$.

The XRD patterns also show that pre-curing of the mixture before 3-roll mill processing results in the most significant decrease of the (110) peak, as compared to the other sample. But the (002) peak does not disappear. Figure 4.16 shows TEM images obtained for this pre-cured sample. Again, multilayer $Ti_3C_2T_x$ sheets can be seen. The intercalation between the layers can also be clearly seen via TEM. Table 4.1 summarizes the shifts in d_{002} spacings observed in this study. Use of RTIL in making the composites causes intercalation between the $Ti_3C_2T_x$ layers of about 4 Å. After application of sufficient shear, the d-spacing increases even further to 5 Å, as a result of intercalation of another material, which is not yet precisely known but suggested to be epoxy.

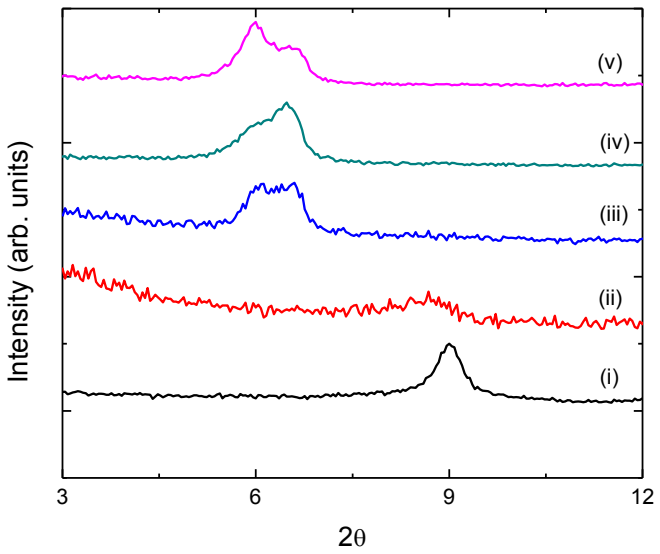

Figure 4.15: XRD patterns zooming in on (002) peaks observed for (i) multilayered $Ti_3C_2T_x$, (ii) 20wt.% $Ti_3C_2T_x$-epoxy composite made with PACM, (iii) 20wt.% $Ti_3C_2T_x$-epoxy-RTIL composite made using 3-roll mill, (iv) 20wt.% $Ti_3C_2T_x$-epoxy-RTIL composite made using rotational mixer, and (v) 20wt.% $Ti_3C_2T_x$ dispersed in pre-cured epoxy-RTIL mixture.

Table 4.1: Shift in the d-spacing of the $Ti_3C_2T_x$ particles after addition of only the RTIL, and after shear processing through the 3-roll mill of the MXene-epoxy-RTIL mixture.

Sample Name	2θ	d_{002} spacing
ML – $Ti_3C_2T_x$	9°	9. 8Å
$Ti_3C_2T_x$ + RTIL	6.5 – 6.7°	13.3 – 13.7Å
$Ti_3C_2T_x$ + RTIL + epoxy	5.95 – 6.0°	14.5 – 14.8Å

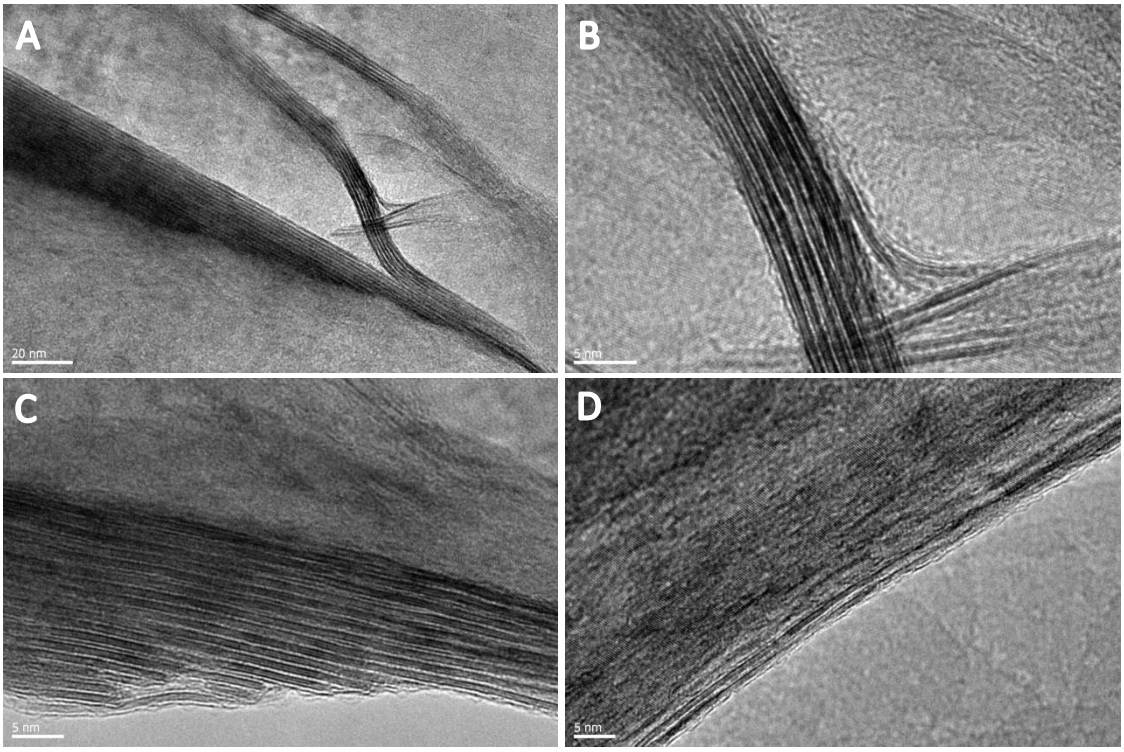

Figure 4.16: (A-D) TEM images for pre-cured 20wt.% $Ti_3C_2T_x$-epoxy-RTIL mixture.

Processing of the $Ti_3C_2T_x$-epoxy-RTIL mixture through a 3-roll mill, despite various enhancements, has not yielded exfoliated flakes of $Ti_3C_2T_x$ dispersed in the epoxy matrix. Even the composite produced using the most promising processing

regimen demonstrates the (002) pea, while the (002) peak should disappear if single layers of $Ti_3C_2T_x$ were dispersed in the matrix.

4.4 Conclusions

The primary conclusion of the study of $Ti_3C_2T_x$-epoxy-RTIL composites is that the $Ti_3C_2T_x$ particles demonstrate interesting interactions with the RTIL solvent. Curing of the mixture, regardless of the mixing technique, yielded intercalation between $Ti_3C_2T_x$ flakes by the epoxy matrix, causing the $Ti_3C_2T_x$ multilayers to swell by more than 4Å. $Ti_3C_2T_x$-epoxy composites that were synthesized without the RTIL did not show this intercalation behavior. The mode of this interaction is most likely the cation of the RTIL interacting with $Ti_3C_2T_x$, which is negatively charged because of its surface terminations. After application of sufficient shear, this initial intercalation allows maybe even epoxy intercalation.

The goal of this study was to create nanocomposites of $Ti_3C_2T_x$ single layers in an epoxy matrix, but this could not be achieved. The application of laminar shear demonstrated exfoliation of graphene layers from graphite powder in a similar study. The failure to achieve this in the study shows that mechanical exfoliation of $Ti_3C_2T_x$ does not solely depend on applied shear stress. Approximately 1 to 50 GPa of laminar shear stresses were applied on the $Ti_3C_2T_x$ layers, to no avail, because of poor shear stress transfer. The particle size of the $Ti_3C_2T_x$ did decrease from being on the order of tens of microns to becoming tens of nanometers large after processing. Promisingly, the pre-cured $Ti_3C_2T_x$-epoxy-RTIL mixture showed a significant decrease in the (110) peak of the final composite. If additional pre-cure is carried out, such that epoxy chains are longer

and have more crosslinks, exfoliation of $Ti_3C_2T_x$ single layers dispersed in epoxy, via this method, is possible. The exfoliation is aided by the initial intercalation of the EMIM-DCN RTIL, and is similar to how solutions of delaminated single-layer flakes of $Ti_3C_2T_x$ in water are obtained. One step involves intercalation by dimethyl sulfoxide (DMSO) followed by addition of water and sonication, to produce a solution of dispersed $Ti_3C_2T_x$ flakes. Similarly, the RTIL intercalates between layers, and after sufficient mechanical processing, the possible intercalation of epoxy and some $Ti_3C_2T_x$ exfoliation occurs.

Chapter 5: Summary and Outlook

In this thesis, the synthesis of MXene-epoxy nanocomposites was investigated. Two different methods of synthesizing the composites were studied. A traditional *in situ* polymerization method, which involved dispersing single layers of MXene in acetone, was used to synthesize Ti_3CNT_x-epoxy composites. The other technique was studied to create a more scalable and streamlined approach of synthesizing $Ti_3C_2T_x$-epoxy composites from multilayered $Ti_3C_2T_x$ sheets, via the application of laminar shear stress.

In the case of the *in situ* polymerization, composites with high loadings of Ti_3CNT_x, by weight up to 90%, were made in order to create an artificial nacre-like structure. The high weight fraction resulted in the synthesis of only small amounts of the material, and the high viscosities of the mixtures inhibited flow meaning composites could not be cured in the shape of molds, but rather as pieces at the bottom of a vial. Nanoindentation results and TEM images showed limited synergy between the filler and the matrix. The Young's modulus of the composite increases as filler loading increases, but this modulus value only approaches that of the pure Ti_3CNT_x film, suggesting poor stress transfer efficiency as no synergy occurs. This shows no covalent bonding between the Ti_3CNT_x flakes and the epoxy exists. Even though some single layer exfoliation was observed, Ti_3CNT_x aggregates were also observed. This process was also time-consuming and energy intensive, which makes this method unsuitable for commercial applications.

Another approach taken involved the application of laminar shear to a mixture of $Ti_3C_2T_x$ multilayers and epoxy in order to exfoliate the filler into single layers. This

method has the promise of being more scalable and streamlined. A room temperature ionic liquid, EMIM-DCN, was used as the dispersant and the curing agent for this system. The results from XRD and TEM show that the laminar shear processing method was unable to exfoliate single layers $Ti_3C_2T_x$, and multilayered particles were still observed. Intercalation of the $Ti_3C_2T_x$ multilayers did occur, and was confirmed by both XRD and TEM. The most likely explanation is that the interaction between the cation of the RTIL and $Ti_3C_2T_x$ occurs, which results in the intercalation of the cation between subsequent layers. The most promising trial using the laminar shear technique required curing some of the epoxy monomer with the RTIL, without completely curing the mixture, so that the larger chains would be better equipped to cleave the $Ti_3C_2T_x$ layers. While single layers of $Ti_3C_2T_x$ were not exfoliated, a large drop in the (110) peak was observed, corresponding to a lowering of the order of the $Ti_3C_2T_x$ particles. The shear stress applied also caused a larger shift in the d-spacing than when only RTIL intercalation occurs, suggesting that maybe even some epoxy has intercalated between layers. But this needs to be studied in more detail.

Outlook

First and foremost, the epoxy monomer and RTIL mixture should be pre-cured to a greater extent, while ensuring that the mixture can still be processed. Passing this mixture through the 3-roll mill may have the most promise in successfully exfoliating $Ti_3C_2T_x$ layers. Moreover, since the RTIL is a latent curing agent, the pre-cured mixture can be left idle without fear of its curing. Next, other methods need to be developed that allow production of epoxy composites with single layers of MXene as the filler. The volatile solvent used in the *in situ* polymerization technique was acetone which has a very

low boiling point, and hence is most suitable to make composites. But this acetone is not viable for some other MXenes, so other solvents for MXenes need to be studied for dispersing MXene flakes in epoxy. The resulting epoxy composites can be tested for used for a wide variety of applications, depending on the property improvements they offer.

Another work that can be conducted in the future is studying the effect of surface terminations of MXenes on the synergy between MXene and the epoxy matrix. This work has shown limited or no covalent bonding between Ti_3CNT_x and the epoxy matrix, and wettability is assumed to be poor. As a result, composites consisting of the MXenes and epoxy will show limited improvements, if the filler acts as a void since no bonding exists. When making fiber reinforced composites, the carbon or glass fibers have to be sized, using a proprietary blend of chemicals, so that bonding between the fiber and matrix is strong. This allows these fiber composites to have significantly improved mechanical performance. Similarly, in order to improve the performance of MXene-epoxy nanocomposites, the surface of the MXenes needs to be sized.

Lastly, the interaction between the RTIL and $Ti_3C_2T_x$, and other MXenes, needs to be evaluated. In this thesis, the $Ti_3C_2T_x$-epoxy-RTIL system did not yield single layered $Ti_3C_2T_x$ dispersed in epoxy. But the proposed interactions between the negatively charge layers of $Ti_3C_2T_x$ and the imidazolium cation of the RTIL, and their intercalation behavior, suggests that the RTIL can be used to delaminate $Ti_3C_2T_x$. Ionic liquids have delaminated graphene before, and if suspensions of single- or few-layer flakes of MXenes in RTIL can be obtained, then more promising MXene-epoxy nanocomposites can be produced as well.

List of References:

1. Goodman, S. H. Handbook of Thermoset Plastics (2nd Edition). William Andrew Publishing/Noyes: **1998**.

2. Castan, P. Process of preparing synthetic resins. **1943**.

3. Throckmorton, James. *Ionic Liquid-Modified Thermosets and Their Nanocomposites: Dispersion, Exfoliation, Degradation, and Cure*. Thesis. Drexel University, 2015. Philadelphia: Drexel U, **2015**.

4. Ratna, D., Handbook of Thermoset Resins. Smithers Rapra Technology: **2009**.

5. Rahmathullah, M. Aflal M., et al. Room temperature ionic liquids as thermally latent initiators for polymerization of epoxy resins. *Macromolecules* **2009,** 42(9), 3219-3221.

6. Maka, H.; Spychaj, T.; Pilawka, R., Epoxy Resin/Ionic Liquid Systems: The Influence of Imidazolium Cation Size and Anion Type on Reactivity and Thermomechanical Properties. *Industrial & Engineering Chemistry Research* **2012,** *51*(14), 5197-5206.

7. Plechkova, N. V.; Seddon, K. R., Applications of ionic liquids in the chemical industry. *Chemical Society Reviews* **2008,** *37* (1), 123-150.

8. Marsh, K. N.; Boxall, J. A.; Lichtenthaler, R., Room temperature ionic liquids and their mixtures—a review. *Fluid Phase Equilibria* **2004,** *219* (1), 93-98.

9. Seddon, K., Room-temperature ionic liquids: neoteric solvents for clean catalysis. *Kinetics and Catalysis* **1995,** *37* (5), 693-697.

10. Kapustinskii, A. F. Lattice energy of ionic crystals. *Quarterly Reviews, Chemical Society* **1956,** 10(3), 283-294.

11. Heise, M. S., and G. C. Martin. Mechanism of 2-ethyl-4-methylimidazole in the curing of the diglycidyl ether of bisphenol A. *Journal of Polymer Science Part C: Polymer Letters* **1988,** 26(3), 153-157.

12. Throckmorton, J.A., et al. Room temperature ionic liquids for epoxy nanocomposite synthesis: direct dispersion and cure. *Composites Science and Technology* **2013,** 86, 38-44.

13. Watters, A.L.; Palmese G.R. Ultralow percolation threshold of single walled carbon nanotube-epoxy composites synthesized via an ionic liquid dispersant/initiator. *Mater. Res. Express* **2014**, 1(3).

14. Throckmorton, J., and Palmese, G.R. Direct preparation of few layer graphene epoxy nanocomposites from untreated flake graphite. *ACS Applied Materials & Interfaces* **2015,** 7(27), 14870-14877.

15. Thostenson, E. T.; Li, C.; Chou, T.-W., Nanocomposites in context. *Composites Science and Technology* **2005,** *65* (3–4), 491-516.

16. Kotsilkova, R., Thermoset Nanocomposites for Engineering Applications. Smithers Rapra Technology: **2007**.

17. Kelly, A., Composites in context. *Composites Science and Technology* **1985,** *23* (3), 171-199.

18. Greenfeld, I.; Wagner, H. D., Nanocomposite toughness, strength and stiffness: role of filler geometry. *Nanocomposites* **2015,** *1* (1), 3-17.

19. Mackay, M. E.; Tuteja, A.; Duxbury, P. M.; Hawker, C. J.; Van Horn, B.; Guan, Z.; Chen, G.; Krishnan, R., General strategies for nanoparticle dispersion. *Science* **2006,** *311* (5768), 1740-1743.

20. Wagner, H. D.; Vaia, R. A., Nanocomposites: issues at the interface. *Materials Today* **2004,** *7* (11), 38-42.

21. Uddin, M. F.; Sun, C. T., Strength of unidirectional glass/epoxy composite with silica nanoparticle-enhanced matrix. *Composites Science and Technology* **2008,** *68* (7–8), 1637-1643.

22. Johnsen, B. B.; Kinloch, A. J.; Mohammed, R. D.; Taylor, A. C.; Sprenger, S., Toughening mechanisms of nanoparticle-modified epoxy polymers. *Polymer* **2007,** *48* (2), 530-541.

23. Wichmann, M. H. G.; Schulte, K.; Wagner, H. D., On nanocomposite toughness. *Composites Science and Technology* **2008,** *68* (1), 329-331.

24. Wagner, H. D.; Ajayan, P. M.; Schulte, K., Nanocomposite toughness from a pull-out mechanism. *Composites Science and Technology* **2013,** *83* (0), 27-31.

25. Norman, D. A.; Robertson, R. E., Rigid-particle toughening of glassy polymers. *Polymer* **2003,** *44* (8), 2351-2362.

26. Kinloch, A. J.; Taylor, A. C., The toughening of cyanate-ester polymers Part I Physical modification using particles, fibres and woven-mats. *J Mater Sci* **2002,** *37* (3), 433-460.

27. Zhang, H.; Zhang, Z.; Friedrich, K.; Eger, C., Property improvements of in situ epoxy nanocomposites with reduced interparticle distance at high nanosilica content. *Acta Materialia* **2006,** *54* (7), 1833-1842.

28. Bauhofer, W.; Kovacs, J. Z., A review and analysis of electrical percolation in carbon nanotube polymer composites. *Composites Science and Technology* **2009,** *69* (10), 1486-1498.

29. Gao, F., Clay/polymer composites: the story. *Materials Today* **2004,** *7* (11), 50-55.

30. Sinha Ray, S.; Okamoto, M., Polymer/layered silicate nanocomposites: a reviewfrom preparation to processing. *Progress in Polymer Science* **2003,** *28* (11), 1539-1641.

31.Bhatnagar, A.; Sain, M., Processing of cellulose nanofiber-reinforced composites. *Journal of Reinforced Plastics and Composites* **2005,** *24* (12), 1259-1268.

32. Hubbe, M. A.; Rojas, O. J.; Lucia, L. A.; Sain, M., Cellulosic nanocomposites: a review. *BioResources* **2008,** *3* (3), 929-980.

33. Eichhorn, S.; Dufresne, A.; Aranguren, M.; Marcovich, N.; Capadona, J.; Rowan, S.; Weder, C.; Thielemans, W.; Roman, M.; Renneckar, S., Review: current international research into cellulose nanofibres and nanocomposites. *Journal of Material Science* **2010,** *45* (1), 1-33.

34. Ma, P.-C.; Siddiqui, N. A.; Marom, G.; Kim, J.-K., Dispersion and functionalization of carbon nanotubes for polymer-based nanocomposites: A review. *Composites Part A: Applied Science and Manufacturing* **2010,** *41* (10), 1345-1367.

35. Rana, S.; Alagirusamy, R.; Joshi, M., A Review on Carbon Epoxy Nanocomposites. *Journal of Reinforced Plastics and Composites* **2009,** *28* (4), 461-487.

36.Li, J.; Kim, J.-K., Percolation threshold of conducting polymer composites containing 3D randomly distributed graphite nanoplatelets. *Composites Science and Technology* **2007,** *67* (10), 2114-2120.

37. Nicolosi, V., Chhowalla, M., Kanatzidis, M. G., Strano, M. S. & Coleman, J. N. Liquid exfoliation of layered materials. *Science* **2013,** 340, 1226419.

38. Fiori, G. et al. Electronics based on two-dimensional materials. *Nature Nanotechnology* **2014** 9, 768–779.

39. Xia, F., Wang, H., Xiao, D., Dubey, M. & Ramasubramaniam, A. Two-dimensional material nanophotonics. *Nature Photonics* **2014,** 8, 899–907.

40. Koppens, F. et al. Photodetectors based on graphene, other two-dimensional materials and hybrid systems. *Nature Nanotechnology* **2014,** 9, 780–793.

41. Akinwande, D., Petrone, N. & Hone, J. Twodimensional flexible nanoelectronics. *Nature Communications* **2014** 5, 5678.

42. Cepellotti, A. et al. Phonon hydrodynamics in twodimensional materials. *Nature Communications* **2015** 6, 6400.

43. Alexandre, M.; Dubois, P., Polymer-layered silicate nanocomposites: preparation, properties and uses of a new class of materials. *Materials Science and Engineering: Reports* **2000,** *28* (1–2), 1-63.

44. Sengupta, R.; Bhattacharya, M.; Bandyopadhyay, S.; Bhowmick, A. K., A review on the mechanical and electrical properties of graphite and modified graphite reinforced polymer composites. *Progress in Polymer Science* **2011,** *36* (5), 638-670.

45. Kuilla, T.; Bhadra, S.; Yao, D.; Kim, N. H.; Bose, S.; Lee, J. H., Recent advances in graphene based polymer composites. *Progress in Polymer Science* **2010,** *35* (11), 1350-1375.

46. Kim, H.; Abdala, A. A.; Macosko, C. W., Graphene/Polymer Nanocomposites. *Macromolecules* **2010,** *43* (16), 6515-6530.

47. Stankovich, S.; Dikin, D. A.; Dommett, G. H. B.; Kohlhaas, K. M.; Zimney, E. J.; Stach, E. A.; Piner, R. D.; Nguyen, S. T.; Ruoff, R. S., Graphene-based composite materials. *Nature* **2006,** *442* (7100), 282-286.

48. Celzard, A.; McRae, E.; Marêché, J. F.; Furdin, G.; Dufort, M.; Deleuze, C., Composites based on micron-sized exfoliated graphite particles: Electrical conduction, critical exponents and anisotropy. *Journal of Physics and Chemistry of Solids* **1996,** *57* (6–8), 715-718.

49. Novoselov, K. S.; Geim, A. K.; Morozov, S. V.; Jiang, D.; Zhang, Y.; Dubonos, S. V.; Grigorieva, I. V.; Firsov, A. A., Electric Field Effect in Atomically Thin Carbon Films. *Science* **2004,** *306* (5696), 666-669.

50. Zou, H.; Wu, S.; Shen, J., Polymer/Silica Nanocomposites: Preparation, Characterization, Properties, and Applications. *Chemical Reviews* **2008,** *108* (9), 3893- 3957.

51. Naguib, M. et al. Two-dimensional nanocrystals produced by exfoliation of Ti3AlC2. *Advanced Materials* **2011,** 23, 4248–4253.

52. Naguib, M. et al. Two-dimensional transition metal carbides. *ACS Nano* **2012,** 6, 1322–1331.

53. Naguib, M., Mochalin, V. N., Barsoum, M. W. & Gogotsi, Y. MXenes: a new family of two-dimensional materials. *Advanced Materials* **2014** 26, 992–1004.

54. Barsoum, M. W. MAX Phases: Properties of Machinable Ternary Carbides and Nitrides (Wiley, **2013**).

55. B. Anasori, M. R. Lukatskaya, Y. Gogotsi, 2D metal carbides and nitrides (MXenes) for energy storage, *Nature Reviews Materials* **2017**, 2, 16098.

56. Naguib, M. et al. New two-dimensional niobium and vanadium carbides as promising materials for Li-ion batteries. *Journal of the American Chemical Society* **2013,** 135, 15966–15969.

57. Ghidiu, M. et al. Synthesis and characterization of two-dimensional Nb4C3 (MXene). *Chemical Communications* **2014,** 50, 9517–9520.

58. Anasori, B. et al. Two-dimensional, ordered, double transition metals carbides (MXenes). *ACS Nano* **2015,** 9, 9507–9516.

59. Urbankowski, P. et al. Synthesis of two-dimensional titanium nitride Ti4N3 (MXene). *Nanoscale* **2016,** 8, 11385–11391.

60. Meshkian, R. et al. Synthesis of two-dimensional molybdenum carbide, Mo2C, from the gallium based atomic laminate Mo2Ga2C. *Scripta Materialia* **2015,** 108, 147–150.

61. Khazaei, M. et al. Novel electronic and magnetic properties of two-dimensional transition metal carbides and nitrides. *Advanced Functional Materials* **2013,** 23, 2185–2192.

62. Ghidiu, M., Lukatskaya, M. R., Zhao, M.-Q., Gogotsi, Y. & Barsoum, M. W. Conductive two-dimensional titanium carbide 'clay' with high volumetric capacitance. *Nature* **2014,** 516, 78–81.

63. Halim, J. et al. Synthesis and characterization of 2D molybdenum carbide (MXene). *Advanced Functional Materials* **2016,** 26, 3118–3127.

64. Zhou, J. et al. A two-dimensional zirconium carbide by selective etching of Al3C3 from nanolaminated Zr3Al3C5. *Angewadte Chemie Int. Ed.* **2016**, 128, 5092–5097.

65. Mashtalir, O. et al. Intercalation and delamination of layered carbides and carbonitrides. *Nature Communications* **2013,** 4, 1716.

66. Mashtalir, O., Lukatskaya, M. R., Zhao, M. Q., Barsoum, M. W. & Gogotsi, Y. Amine-assisted delamination of Nb2C MXene for Li-Ion energy storage devices. *Advanced Materials* **2015,** 27, 3501–3506.

67. Naguib, M., Unocic, R. R., Armstrong, B. L. & Nanda, J. Large-scale delamination of multi-layers transition metal carbides and carbonitrides MXenes. *Dalton Transactions* **2015,** 44, 9353–9358.

68. Lipatov, A. et al. Effect of synthesis on quality, electronic properties and environmental stability of individual monolayer Ti3C2 MXene flakes. *Advanced Electronic Materials* **2016,** 2, 1600255.

69. Wang, X. et al. Pseudocapacitance of MXene nanosheets for high-power sodium-ion hybrid capacitors. *Nature Communications* **2015,** 6, 6544.

70. Dall'Agnese, Y., Taberna, P. L., Gogotsi, Y. & Simon, P. Two-dimensional vanadium carbide (MXene) as positive electrode for sodium-ion capacitors. *Journal of Physical Chemistry Letters* **2015,** 6, 2305–2309.

71. Boota, M. et al. Pseudocapacitive electrodes produced by oxidant-free polymerization of pyrrole between the layers of 2D titanium carbide (MXene). *Advanced Materials* **2016,** 28, 1517–1522.

72. Shahzad, F. et al. Electromagnetic interference shielding with 2D transition metal carbides (MXenes) *Science* **2016,** 353, 1137–1140.

73. Ling, Z. et al. Flexible and conductive MXene films and nanocomposites with high capacitance. *Proc. Natl Acad. Sci. USA* **2014,** 111, 16676–16681.

74. Zhang, H. et al. Preparation, mechanical and antifriction performance of MXene/polymer composites. *Mater. Des.* **2016,** 92, 682–689.

75. Peng, Q. et al. Unique lead adsorption behavior of activated hydroxyl group in two-dimensional titanium carbide. *Journal of the American Chemical Society* **2014,** 136, 4113–4116.

76. Zou, G. et al. Synthesis of urchin-like rutile titania carbon nanocomposites by iron-facilitated phase transformation of MXene for environmental remediation. *Journal of Materials Chemistry A* **2016,** 4, 489–499.

77. Guo, J., Peng, Q., Fu, H., Zou, G. & Zhang, Q. Heavymetal adsorption behavior of two-dimensional alkalization-intercalated MXene by first-principles calculations. *Journal of Physical Chemistry C* **2015**, 119, 20923–20930.

78. Mashtalir, O. et al. Dye adsorption and decomposition on two-dimensional titanium carbide in aqueous media. *Journal of Materials Chemistry A* **2014,** 2, 14334–14338.

79. Seh, Z. W. et al. Two-dimensional molybdenum carbide (MXene) as an efficient electrocatalyst for hydrogen evolution. *ACS Energy Letters* **2016,** 1, 589–594.

80. Ma, T. Y., Cao, J. L., Jaroniec, M. & Qiao, S. Z. Interacting carbon nitride and titanium carbide nanosheets for high-performance oxygen evolution. *Angewadte Chemie Int. Ed.* **2015,** 55, 1138–1142.

81. Potts JR, Dreyer DR, Bielawski CW, Ruoff RS. Graphene-based polymer nanocomposites. *Polymer* **2011**, 7;52(1):5-25.

82. Zou, H.; Wu, S.; Shen, J., Polymer/Silica Nanocomposites: Preparation, Characterization, Properties, and Applications. *Chemical Reviews* **2008,** *108* (9), 3893-3957.

83. Kuilla, T.; Bhadra, S.; Yao, D.; Kim, N. H.; Bose, S.; Lee, J. H., Recent advances in graphene based polymer composites. *Progress in Polymer Science* **2010,** *35* (11), 1350-1375.

84. Kim, H.; Abdala, A. A.; Macosko, C. W., Graphene/Polymer Nanocomposites. *Macromolecules* **2010,** *43* (16), 6515-6530.

85. Stankovich, S.; Dikin, D. A.; Dommett, G. H. B.; Kohlhaas, K. M.; Zimney, E. J.; Stach, E. A.; Piner, R. D.; Nguyen, S. T.; Ruoff, R. S., Graphene-based composite materials. *Nature* **2006,** *442* (7100), 282-286.

86. Krishnamoorti, R., Strategies for Dispersing Nanoparticles in Polymers. *MRS Bulletin* **2007,** *32* (04), 341-347.

87. Viswanathan, V.; Laha, T.; Balani, K.; Agarwal, A.; Seal, S., Challenges and advances in nanocomposite processing techniques. *Materials Science and Engineering: Reports* **2006,** *54* (5–6), 121-285.

88. Tang, Long-Cheng, et al. The effect of graphene dispersion on the mechanical properties of graphene/epoxy composites. *Carbon* **2013,** 60, 16-27.

88. Park, S.; Ruoff, R. S., Chemical methods for the production of graphenes. *Nature Nanotechnology* **2009,** *4* (4), 217-224.

89. Kuila, T.; Bose, S.; Mishra, A. K.; Khanra, P.; Kim, N. H.; Lee, J. H., Chemical functionalization of graphene and its applications. *Progress in Materials Science* **2012,** *57* (7), 1061-1105.

90. Rafiee, Mohammad A., et al. Enhanced mechanical properties of nanocomposites at low graphene content. *ACS Nano **2009***, 3(12), 3884-3890.

91. Liang, Jiajie, et al. Electromagnetic interference shielding of graphene/epoxy composites. *Carbon* 2009, 47(3), 922-925.

92. Fang, Ming, et al. Constructing hierarchically structured interphases for strong and tough epoxy nanocomposites by amine-rich graphene surfaces. *Journal of Materials Chemistry **2010***, 20(43), 9635-9643.

93. Wang, Xin, et al. Covalent functionalization of graphene with organosilane and its use as a reinforcement in epoxy composites. *Composites Science and Technology* 2012, 72(6), 737-743.

94. Teng, Chih-Chun, et al. Thermal conductivity and structure of non-covalent functionalized graphene/epoxy composites. *Carbon* **2011,** 49(15), 5107-5116.

95. Song, Sung Ho, et al. Enhanced Thermal Conductivity of Epoxy–Graphene Composites by Using Non-Oxidized Graphene Flakes with Non-Covalent Functionalization. *Advanced Materials* **2013,** 25(5), 732-737.

96. Li, J.; Sham, M. L.; Kim, J.-K.; Marom, G., Morphology and properties of UV/ozone treated graphite nanoplatelet/epoxy nanocomposites. *Composites Science and Technology* **2007,** *67* (2), 296-305.

97. Yasmin, A.; Luo, J.-J.; Daniel, I. M., Processing of expanded graphite reinforced polymer nanocomposites. *Composites Science and Technology* **2006,** *66* (9), 1182-1189.

98. Yu, Aiping, et al. Enhanced thermal conductivity in a hybrid graphite nanoplatelet–carbon nanotube filler for epoxy composites. *Advanced Materials* **2008,** 20(24), 4740-4744.

99. Jović, N.; Dudić, D.; Montone, A.; Antisari, M. V.; Mitrić, M.; Djoković, V., Temperature dependence of the electrical conductivity of epoxy/expanded graphite nanosheet composites. *Scripta Materialia* **2008,** *58* (10), 846-849.

100. Li, J.; Kim, J.-K.; Lung Sham, M., Conductive graphite nanoplatelet/epoxy nanocomposites: Effects of exfoliation and UV/ozone treatment of graphite. *Scripta Materialia* **2005,** *53* (2), 235-240.

101. Ganguli, S.; Roy, A. K.; Anderson, D. P., Improved thermal conductivity for chemically functionalized exfoliated graphite/epoxy composites. *Carbon* **2008,** *46* (5), 806-817.

102. Debelak, B.; Lafdi, K., Use of exfoliated graphite filler to enhance polymer physical properties. *Carbon* **2007,** *45* (9), 1727-1734.

103. Rafiee, Mohammed A., et al. Fracture and fatigue in graphene nanocomposites. *Small* 2010, 6(2), 179-183.

104. Yu, Aiping, et al. Graphite nanoplatelet− epoxy composite thermal interface materials. *The Journal of Physical Chemistry C* 2007, 111(21), 7565-7569.

105. Liu, N.; Luo, F.; Wu, H.; Liu, Y.; Zhang, C.; Chen, J., One-Step Ionic-Liquid- Assisted Electrochemical Synthesis of Ionic-Liquid-Functionalized Graphene Sheets Directly from Graphite. *Advanced Functional Materials* **2008,** *18* (10), 1518-1525.

106. Lu, J.; Yang, J.-x.; Wang, J.; Lim, A.; Wang, S.; Loh, K. P., One-Pot Synthesis of Fluorescent Carbon Nanoribbons, Nanoparticles, and Graphene by the Exfoliation of Graphite in Ionic Liquids. *ACS Nano* **2009,** *3* (8), 2367-2375.

107. Wang, X.; Fulvio, P. F.; Baker, G. A.; Veith, G. M.; Unocic, R. R.; Mahurin, S. M.; Chi, M.; Dai, S., Direct exfoliation of natural graphite into micrometre size few layers graphene sheets using ionic liquids. *Chemical Communications* **2010,** *46* (25), 4487-4489.

108. Kislenko, S. A.; Samoylov, I. S.; Amirov, R. H., Molecular dynamics simulation of the electrochemical interface between a graphite surface and the ionic liquid [BMIM][PF6]. *Physical Chemistry Chemical Physics* **2009,** *11* (27), 5584-5590.

109. Wang, J.; Chu, H.; Li, Y., Why Single-Walled Carbon Nanotubes Can Be Dispersed in Imidazolium-Based Ionic Liquids. *ACS Nano* **2008,** *2* (12), 2540-2546.

110. Jackson, A. P., J. F. V. Vincent, and R. M. Turner. The Mechanical Design of Nacre. *Proceedings of the Royal Society B: Biological Sciences* **1988,** 234(1277), 415-40.

111. Wang, R. Z., Z. Suo, A. G. Evans, N. Yao, and I. A. Aksay. Deformation Mechanisms in Nacre. *Journal of Materials Research***2001**, 16(09), 2485-493.

112. Tang, Zhiyong, Nicholas A. Kotov, Sergei Magonov, and Birol Ozturk. Nanostructured Artificial Nacre. *Nature Materials* **2003,** 2(6), 413-18.

113. Tan, Zhibing, Miao Zhang, Chun Li, Shiyong Yu, and Gaoquan Shi. A General Route to Robust Nacre-Like Graphene Oxide Films. *ACS Applied Materials & Interfaces* **2015,** 7(27), 15010-5016.

114. Wan, Sijie, Yuchen Li, Jingsong Peng, Han Hu, Qunfeng Cheng, and Lei Jiang. Synergistic Toughening of Graphene Oxide-Molybdenum Disulfide-Thermoplastic Polyurethane Ternary Artificial Nacre. *ACS Nano* **2015,** 9(1), 708-14.

115. Zeng, Xiaoliang, Lei Ye, Shuhui Yu, Hao Li, Rong Sun, Jianbin Xu, and Ching-Ping Wong. Artificial Nacre-like Papers Based on Noncovalent Functionalized Boron Nitride Nanosheets with Excellent Mechanical and Thermally Conductive Properties. *Nanoscale* **2015,** 7(15), 6774-781.

116. Maleski, Kathleen, Vadym N. Mochalin, and Yury Gogotsi. Dispersions of Two-Dimensional Titanium Carbide MXene in Organic Solvents. *Chemistry of Materials* **2017**, 29(4), 1632-1640.

117. Xia, Z. Y., et al., The Exfoliation Of Graphene In Liquids By Electrochemical, Chemical, And Sonication-Assisted Techniques: A Nanoscale Study. *Advanced Functional Materials* **2013**, 23 (37), 4684-4693.

118. Łoś, S., et al., Cleavage And Size Reduction Of Graphite Crystal Using Ultrasound Radiation. *Carbon* **2013**, 55 (0), 53-61.

119. Guiáshang, N., Controllable Selective Exfoliation Of High-Quality Graphene Nanosheets And Nanodots By Ionic Liquid Assisted Grinding. *Chemical Communications* **2012**, 48 (13), 1877-1879.

120. Wakabayashi, K., et al., Polypropylene-Graphite Nanocomposites Made By Solid-State Shear Pulverization: Effects Of Significantly Exfoliated, Unmodified Graphite Content On Physical, Mechanical And Electrical Properties. *Polymer* **2010**, 51 (23), 5525-5531.

121. León, V.; Rodriguez, A. M.; Prieto, P.; Prato, M.; Vázquez, E., Exfoliation Of Graphite With Triazine Derivatives Under Ball-Milling Conditions: Preparation Of Few- Layer Graphene Via Selective Noncovalent Interactions. *ACS Nano* **2013**, 8 (1), 563-571.

122. Leon, V., et al., Few-Layer Graphenes From Ball-Milling Of Graphite With Melamine. *Chemical Communications* **2011**, 47 (39), 10936-10938.

123. Bang, J. H.; Suslick, K. S., Applications Of Ultrasound To The Synthesis Of Nanostructured Materials. *Advanced Materials* **2010**, 22 (10), 1039-1059.

124. Suslick, K. S., Sonochemistry. *Science* **1990**, 247, 1439-1445.

125. Chen, J.; Duan, M.; Chen, G., Continuous Mechanical Exfoliation Of Graphene Sheets Via Three-Roll Mill. *Journal of Materials Chemistry* **2012**, 22 (37), 19625-19628.

126. Yasmin, A.; Daniel, I. M., Mechanical And Thermal Properties Of Graphite Platelet/Epoxy Composites. *Polymer* **2004**, 45 (24), 8211-8219.

127. Thostenson, E. T.; Ziaee, S.; Chou, T.-W., Processing And Electrical Properties Of Carbon Nanotube/Vinyl Ester Nanocomposites. *Composites Science and Technology* **2009**, 69 (6), 801-804.

128. Hu, Tao, et al. "Interlayer coupling in two-dimensional titanium carbide MXenes." *Physical Chemistry Chemical Physics* **2016,** 18(30), 20256-20260.

129. Soule, D. E.; Nezbeda, C. W., Direct Basal-Plane Shear In Single-Crystal Graphite. *Journal of Applied Physics* **1968**, 39 (11), 5122-5139.

130. Liu, Z.; Zhang, S.-M.; Yang, J.-R.; Liu, J.; Yang, Y.-L.; Zheng, Q.-S., Interlayer Shear Strength Of Single Crystalline Graphite. *Acta Mechanica Sinica* **2012**, 28 (4), 978-982.

131. Jogun, S.; Zukoski, C. F., Rheology Of Dense Suspensions Of Platelike articles. *Journal of Rheology* **1996**, 40 (6), 1211-1232.

132. Jäckel, Nicolas, et al. "Electrochemical in situ tracking of volumetric changes in two-dimensional metal carbides (MXenes) in ionic liquids." *ACS Applied Materials & Interfaces* **2016**, 8(47), 32089-32093.